

---

# Conservative Continuous-Time Treatment Optimization

---

Nora Schneider<sup>\*123</sup> Georg Manten<sup>\*123</sup> Niki Kilbertus<sup>123</sup>

## Abstract

We develop a conservative continuous-time stochastic control framework for treatment optimization from irregularly sampled patient trajectories. The unknown patient dynamics are modeled as a controlled stochastic differential equation with treatment as a continuous-time control. Naive model-based optimization can exploit model errors and propose out-of-support controls, so optimizing the estimated dynamics may not optimize the true dynamics. To limit extrapolation, we add a consistent signature-based MMD regularizer on path space that penalizes treatment plans whose induced trajectory distribution deviates from observed trajectories. The resulting objective minimizes a computable upper bound on the true cost. Experiments on benchmark datasets show improved robustness and performance compared to non-conservative baselines.

## 1. Introduction

A key challenge in healthcare is finding the best treatment plan to guide patient trajectories toward a desired clinical outcome, such as selecting a chemotherapy dosing schedule that maximally reduces tumor size. Unlike a one-shot decision, treatment is inherently temporal and continuous. Patient state evolves constantly, measurements are taken irregularly, and interventions are applied over time. Designing optimal plans therefore requires a model that can estimate potential future patient trajectories under candidate treatment plans, including ones never administered before.

Historically, this has been approached by mechanistic continuous-time models, such as pharmacokinetic differential equations. These often manually prescribed and hard-earned mathematical models are interpretable and continuous by design, but are often still overly simplistic and fail

---

<sup>\*</sup>Equal contribution <sup>1</sup>Technical University of Munich <sup>2</sup>Helmholtz Munich <sup>3</sup>Munich Center for Machine Learning. Correspondence to: Nora Schneider <nora.schneider@tum.de>, Georg Manten <georg.manten@tum.de>, Niki Kilbertus <niki.kilbertus@tum.de>.

to capture the complex and stochastic dynamics found in heterogeneous patient settings. Flexible data-driven methods from machine learning, in particular causal inference, promise to overcome these limitations. However, most of these methods operate in discrete time with fixed decision points (and often finite actions), which does not account for the continuous and irregular nature of clinical reality.

In high stakes decisions, we often cannot perform direct experimentation due to practical or ethical considerations. Therefore, one is typically constrained to an offline setting: given observed trajectories collected under existing treatment plans, we aim to design future treatment plans that ideally perform better than historical ones. In this offline setting, when first learning the system’s dynamics and then optimizing over that model, the optimization may act adversarially by finding and exploiting model errors—in particular erroneous extrapolation behavior in data-poor regions. This problem, well known in offline RL, is severely exacerbated in continuous-time treatment planning, where actions live in path space. The classical overlap (or positivity) assumption, already challenging in discrete settings, becomes practically impossible to satisfy.

In this paper, we develop a principled method for *conservative optimization of continuous-time treatments from irregularly sampled observational trajectories*. We model patient dynamics as a controlled stochastic differential equation with treatment as a continuous-time control, learn this model from data, and conservatively penalize deviation between model-induced and observed trajectory distributions via a signature-kernel conditional MMD on path space, when optimizing treatments.

## 2. Related Work

**Continuous-Time Longitudinal Causal Inference.** Motivated by these limitations, machine learning—more specifically causal inference—has proposed flexible data-driven techniques for longitudinal treatment effect estimation by extending ideas from the potential outcomes framework. Recent work includes extensions to continuous-time settings that handle irregular observations, event-driven dynamics, and time-dependent confounding, but do not offer a principled way to optimize treatment plans from finite observational data. Some methods focus on population-level

outcomes, unable to condition on patient-specific history, which prevents predicting personalized responses to candidate treatment plans (Sun & Crawford, 2022; Ying, 2025; Lok, 2008; Schulam & Saria, 2017; Hızlı et al., 2023). Other approaches condition on patient history via neural ODEs or neural CDEs, but typically model treatments as categorical variables applied at discrete decision times (De Brouwer et al., 2022; Seedat et al., 2022; Hess et al., 2023; Hess & Feuerriegel, 2025). The INSITE-framework (Kacprzyk et al., 2024) models continuous-valued treatments as controls in the governing differential equations for treatment effect estimation.

Although these methods are identifiable under continuous-time extensions of standard potential-outcomes assumptions in the infinite-sample limit, they rely on overlap/positivity, which is already fragile in discrete settings (D’Amour et al., 2021). In continuous time, finite data make this issue substantially worse: covering all treatments at all times for all histories is impossible, so optimization can select plans that drive the state-treatment trajectory far outside the empirical support, where estimates may become unreliable.

Overall, existing works stop at estimation and do not optimize treatments, often consider treatment as categorical and/or applied only at discrete event times preventing them from discovering new continuous-time controls, and when naively optimized over, may suffer from large extrapolation error due to poor overlap.

**Optimal Dynamic Treatment Regimes (DTR)** learn a sequence of history-dependent decision rules that map patient information at each decision point to a treatment to optimize expected clinical outcomes (Murphy, 2003; Robins, 2004; Chakraborty & Murphy, 2014; Li et al., 2023; Tsirtsis & Rodriguez, 2023). Most of this literature is formulated in discrete time with fixed decision points, and is often developed with sequential decision making (and sometimes adaptive data collection) in mind rather than personalized planning from a fixed observational dataset. Offline variants exist – for example, Zhou et al. (2023) propose a pessimistic Bayesian Q-learning approach for learning DTRs from observational data, and Wang et al. (2025) propose variational counterfactual intervention planning – but remain discrete-time frameworks. As a result, existing DTR approaches do not address irregular observation schedules typical in clinical time series, where measurements and treatment adjustments occur at non-uniform times. Xu & Zhang (2024) instead learn a joint model not only over dosage values, but also dosage times, while still fundamentally considering a discrete sequence of events rather than a continuous-time control problem.

**Offline Reinforcement Learning (RL)** has also developed ideas around pessimism and uncertainty-aware regularization to prevent model exploitation in discrete Markov de-

cision processes (MDP) (Yu et al., 2020; Kidambi et al., 2020; Yu et al., 2021), also extended to truncating trajectories depending on model uncertainty (Zhang et al., 2023). Again, existing works focus on discrete settings and do not transfer to continuous-time with irregular observations and do not have to grapple with the identification of potential outcomes in our setting. Perhaps most closely related to our work is the approach by Koprulu et al. (2025), who propose a neural stochastic differential equation model to explicitly capture both aleatoric and epistemic model uncertainty. They truncate/penalize rollouts based on implicit, local model uncertainty. Unlike their approach, we do not rely directly on model uncertainty, but consistently penalize distributional mismatch of trajectories induced by a candidate treatment and the observed distribution.

**Our main contributions include:**

- We formalize personalized, continuous-time, offline treatment optimization from irregular observations within a stochastic control framework built on controlled SDEs.
- We derive a conservative planning objective that upper bounds the true cost via conditional integral probability metrics on path space.
- We develop a practically tractable and consistent implementation of this regularizer via a signature-kernel conditional MMD penalizing out-of-support treatment plans to avoid model exploitation.
- We demonstrate empirically that our method outperforms non-conservative baselines in performance and reliability.

**3. Problem Setting**

We consider the problem of finding optimal treatment plans that guide patient trajectories toward desirable outcomes from a causal perspective.

**Setup.** Throughout this paper, let  $I = [t_s, t_f] \subset \mathbb{R}$  be a compact time interval,  $(\Omega, \mathcal{F}, \mathbb{F}, P)$  a complete filtered probability space with filtration  $\mathbb{F} = (\mathcal{F}_t)_{t \in I}$ . On this space, we consider stochastic processes  $U : I \times \Omega \rightarrow A \subseteq \mathbb{R}^{d_u}$  called the *treatment process* (e.g., chemotherapy),  $Y : I \times \Omega \rightarrow \mathbb{R}^{d_y}$  the *outcome process* (e.g., tumor volume) and  $Z : I \times \Omega \rightarrow \mathbb{R}^{d_z}$  denotes time-varying covariates (e.g., biomarkers), compactly denoted in the combined process  $X = (Z, Y) : I \times \Omega \rightarrow \mathbb{R}^{d_x}$ , where  $d_x = d_y + d_z$ , called *state process*. For a fixed treatment plan  $u : I \rightarrow A \subseteq \mathbb{R}^{d_u}$ ,  $X^{(u, \text{pot})} = (X_t^{(u, \text{pot})})_{t \in I}$  is the *potential state process under u*, i.e., the trajectory that would be observed if the treatment were externally set to follow  $u$  over the entire interval  $I$ . For a stochastic process, we write  $X_{[t_1, t_2]}$  for the restriction of  $X$  to  $[t_1, t_2]$ , viewed as a path-valued random variable (RV)  $\Omega \rightarrow (\mathbb{R}^{d_x})^{[t_1, t_2]}$ , denote its law by

$P_{X_{[t_1, t_2]}} = P \circ X_{[t_1, t_2]}^{-1} \in \mathcal{M}_1((\mathbb{R}^{d_x})^{[t_1, t_2]})$  and write  $X = \{X_t\}_{t \in I}$  for the associated family of time-indexed RVs.<sup>1</sup> In addition, the *filtration* of  $X$  is  $\mathcal{F}^X = (\mathcal{F}_t^X)_{t \in I}$ ,  $\mathcal{F}_t^X = \sigma(X_{[t']}) \mid t_s \leq t' \leq t$  and we often write  $P_{Y|X_{[t_1, t_2]}} = P_{Y|\mathcal{F}_{t_1, t_2}^X}$ , where  $\mathcal{F}_{t_1, t_2}^X = \sigma(X_t \mid t_1 \leq t \leq t_2)$ . We use lowercase letters for sample-path realizations, e.g.,  $x = (X_t(\omega))_{t \in I}$  for  $\omega \in \Omega$ .

**Data.** We observe  $N$  i.i.d. patient trajectories. For each patient  $i$ , measurements are recorded at a finite, irregular time grid  $t_s \leq t_1^{(i)} < \dots < t_{n_i}^{(i)} \leq t_f$ , which may differ across patients. At each time point  $t_j^{(i)}$  we observe the triplet  $(Z_{t_j^{(i)}}^{(i)}, Y_{t_j^{(i)}}^{(i)}, U_{t_j^{(i)}}^{(i)})$ . We denote the dataset by  $\mathcal{D} = \{(z^{(i)}, y^{(i)}, u^{(i)})\}_{i=1}^N$ , where  $z^{(i)} = \{(t_j^{(i)}, z_j^{(i)})\}_{j=1}^{n_i}$ ,  $y^{(i)} = \{(t_j^{(i)}, y_j^{(i)})\}_{j=1}^{n_i}$ , and  $u^{(i)} = \{(t_j^{(i)}, u_j^{(i)})\}_{j=1}^{n_i}$  consist of time-value tuples.

**Objective.** Consider a patient of interest at decision time  $t_0 \in I$ . Given the available information up to  $t_0$  (i.e.,  $\mathcal{F}_{t_0}$ ), we aim to find an optimal treatment plan  $u^* : [t_0, t_f] \rightarrow \mathbb{R}^{d_u}$  that minimizes the following function of the potential state process  $(X_t^{(u, \text{pot})})_{t \in [t_0, t_f]}$

$$\min_{u \in \mathcal{U}_{\text{adm}}} \mathbb{E} \left[ \int_{t_0}^{t_f} f(t, X_t^{(u, \text{pot})}, u_t) dt + g(X_{t_f}^{(u, \text{pot})}) \mid \mathcal{F}_{t_0} \right] \quad (1)$$

where  $f : I \times \mathbb{R}^{d_x} \times A \rightarrow \mathbb{R}$  and  $g : \mathbb{R}^{d_x} \rightarrow \mathbb{R}$  are running and terminal cost functions, respectively,  $\mathcal{U}_{\text{adm}}$  is the class of admissible treatment plans, which we specify later.

## 4. Methodology

Our objective in Equation (1) poses two key challenges: (a) Potential state trajectories  $X^{(u, \text{pot})}$  are challenging to estimate from observational data, because they model hypothetical scenarios that cannot be observed simultaneously (Imbens & Rubin, 2015). We address this with a structural dynamics model and approximate it from observational data; we then show which assumptions on the treatment process warrant identification of potential state trajectories (Section 4.1). (b) Optimizing over treatment plans from observational data is challenging because the data consists of historical treatment plans only. When evaluating new treatment plans, any learned model for the potential state process must extrapolate, and predictions may be inaccurate due to model error. When optimized over, these errors can be exploited, resulting in suboptimal treatment plans. We address this and propose an augmented objective that regularizes deviation from the observed trajectory distribution, resulting in a conservative upper bound on the performance of the selected treatment plan (Section 4.2).

<sup>1</sup> $\mathcal{M}_1(\bullet)$  is the set of all probability measures on  $\bullet$ ,  $(\mathbb{R}^{d_x})^{[t_1, t_2]}$  the set of maps from set  $[t_1, t_2]$  to set  $\mathbb{R}^{d_x}$ .

### 4.1. Structural Dynamics Model for Identifiability

We model the patient state as solutions of a controlled stochastic dynamical system, with treatment as the control input. This structural model gives mathematical meaning to potential state trajectories for deterministic plans and, with standard assumptions on the treatment process, connects these potential outcomes to the observational data distribution. Technical details are deferred to Appendix B.

**Assumption 4.1** (Structural Dynamics Model). The observed state process  $X = (X_t)_{t \in I}$  evolves under the (possibly stochastic) treatment process  $U = (U_t)_{t \in I}$  as

$$dX_t = \mu(X_t, U_t) dt + \sigma(X_t, U_t) dW_t, \quad (2)$$

where  $X_0 \sim \mu_0 \in \mathcal{M}_1(\mathbb{R}^{d_x})$ ,  $W = (W_t)_{t \in I}$  a standard  $d_w$ -dimensional Wiener process and  $\mu$  and  $\sigma$  the measurable drift and diffusion functions. For a deterministic plan  $u : I \rightarrow A$ , we define  $X^{(u, \text{pot})}$  as the solution of Equation (2) with  $U_t = u_t$  for all  $t \in I$  and  $X_0^{(u, \text{pot})} \sim \mu_0$ .

We further assume that  $(\mu, \sigma)$  in Equation (2) satisfy the standard regularity conditions (i.e., global-Lipschitz and linear growth assumption) ensuring existence and pathwise uniqueness of a strong solution to the above controlled SDE. Details can be found in Appendix B. With the structural dynamics model, the observed state trajectories are recovered by the potential process under the realized, observed treatment plan, meaning  $X = X^{(U, \text{pot})}$  a.s., as they share the same underlying stochastic dynamics  $(\mu, \sigma, W)$  and only differ through the sampled plan  $u$  and initialization  $x_0$ . With  $\mathbb{F} = (\mathcal{F}_t)_{t \in I}$  being the (completed, right-continuous) filtration generated by the observed processes  $(X, U)$ , i.e.,  $\mathcal{F}_t := \sigma(X_{[t_0, t]}, U_{[t_0, t]})$ , we make the following two assumptions on the treatment process  $U$  following Ying (2025).

**Assumption 4.2** (Full conditional randomization). There exists a bounded function  $\varepsilon(t, \eta) > 0$  such that  $\int_{t_0}^{t_f} \varepsilon(t, \eta) dt \rightarrow 0$  as  $\eta \downarrow 0$ , and for all  $t \in I$ ,  $\eta > 0$ ,

$$\sup_{u \in \mathcal{U}_{\text{adm}}} \mathbb{E} \left[ \left\| P_{X_{[t, t_f]}^{(u, \text{pot})} | U_{[t_0, t+\eta]}, \mathcal{F}_t} - P_{X_{[t, t_f]}^{(u, \text{pot})} | \mathcal{F}_t} \right\|_{\text{TV}} \right] \leq \varepsilon(t, \eta),$$

where  $\|\cdot\|_{\text{TV}}$  denotes total variation distance on the relevant path space.

We can read Assumption 4.2 as the continuous-time analogue of “no unmeasured confounding”. Next, we also extend the typical overlap/positivity assumption to continuous-time.

**Assumption 4.3** (Positivity (Overlap)). Let  $P$  denote the observational law of the joint trajectory  $(X_{[t_0, t_f]}, U_{[t_0, t_f]})$  on the corresponding product path space (with its canonical

$\sigma$ -field). For each plan  $u \in \mathcal{U}_{\text{adm}}$ , let  $P^{(u)}$  denote the interventional law of the joint trajectory  $(X_{[t_0, t_f]}^{(u, \text{pot})}, u_{[t_0, t_f]})$  obtained by fixing the treatment input to  $u$ . Assume that for every  $u \in \mathcal{U}$ ,

$$P^{(u)} \lll P.$$

meaning that events  $B$  on path space, that are impossible in the observed data ( $P(B) = 0$ ), are also impossible under the intervention data ( $(P^{(u)}(B) = 0)$ ).

We already argued that, even though required for rigorous identification statements, overlap is extremely fragile if not practically impossible in continuous-time settings. This is a key motivation for our practical, finite sample remedy of penalizing treatment plans that have zero probability under the observed law.

Finally, in contrast to [Ying \(2025\)](#), we do not assume that the true data-generating process is known, but instead we make the following assumption about the chosen model being well-specified.

**Assumption 4.4** (Distribution). There exist a parameter  $\theta^*$  with  $(\mu_{\theta^*} = \mu, \sigma_{\theta^*} = \sigma)$  (the functions of our structural dynamics model) such that for every  $u \in \mathcal{U}_{\text{adm}}$

$$dX_t^{(u, \text{pot})} = \mu_{\theta^*}(X_t^{(u, \text{pot})}, u_t) dt + \sigma_{\theta^*}(X_t^{(u, \text{pot})}, u_t) dW_t$$

is well-defined and  $(\mu_{\theta^*}, \sigma_{\theta^*})$  can be estimated consistently from the observational law  $P_{X,U}$ . Importantly, we restrict  $\mathcal{U}_{\text{adm}}$  to controls for which the induced law  $P^{(u)}$  satisfies the positivity condition.

*Remark 4.5* (Neural SDEs). In *neural SDEs*,  $\mu_{\theta}$  and  $\sigma_{\theta}$  are parameterized by neural networks and fit  $\theta$  from observational trajectories. For a rich enough model class and a consistent estimator, [Assumption 4.4](#) holds. A sufficient condition that helps ensure that  $P^{(u)} \lll P$  holds is that  $\sigma\sigma^\top$  is independent of  $u$ .

We can now leverage [Ying \(2025, Theorem 1\)](#) to identify the target value when considering deterministic plans for stochastic interventions assigning probability one to path  $u$ :

**Proposition 4.6** (Identifiability). *Under assumptions [Assumptions 4.2 to 4.4](#) and the structural dynamics [Assumption 4.1](#) such that  $X = X^{(U, \text{pot})}$  a.s.,*

$$\mathcal{J}(t_0, X^{(u, \text{pot})}, u) := \mathbb{E} \left[ \nu(X^{(u, \text{pot})}, u) \mid \mathcal{F}_{t_0} \right],$$

is identifiable from the observational law. In particular, for

$$\nu(X^{(u, \text{pot})}, u) = \int_{t_0}^{t_f} f(t, X_t^{(u, \text{pot})}, u_t) dt + g(X_{t_f}^{(u, \text{pot})}).$$

the value  $\mathcal{J}(t_0, X^{(u, \text{pot})}, u)$  is identified.

In the following, we denote by  $X^{(t_0, x_0, u)}$  the (strong) solution of [Equation \(2\)](#) on  $I$  under a deterministic treatment plan  $u$  and initial condition  $X_{t_0} = x_0$ , whose existence and uniqueness are ensured by the regularity conditions in [Appendix B](#). In particular, the induced state process of [Equation \(2\)](#) satisfies the flow property: for any  $\tau \geq t_0$ ,  $X_t^{(t_0, x_0, u)} = X_t^{(\tau, X_\tau^{(t_0, x_0, u)}, u)}$  a.s., equivalently meaning that  $X$  is Markov: conditioned on the current state (and the future control values), the future evolution is independent of the history. Thus, instead of conditioning on the full information  $\mathcal{F}_{t_0}$  it suffices to condition on  $(X_{t_0}, U_{t_0})$ .

Under [Assumptions 4.1 to 4.3](#), we can rewrite the treatment-optimization problem in [Equation \(1\)](#) as a stochastic control problem over the class of admissible controls  $\mathcal{U}_{\text{adm}}$  and finite time horizon  $[t_0, t_f]$  as

$$u^* := \arg \min_{u \in \mathcal{U}_{\text{adm}}} \mathbb{E} \left[ \underbrace{\int_{t_0}^{t_f} f(t, X_t^{(t_0, x_0, u)}, u_t) dt + g(X_{t_f}^{(t_0, x_0, u)})}_{=: \mathcal{J}(t_0, X^{(t_0, x_0, u)}, u)} \right]. \quad (3)$$

We refer to [Appendix B](#) for regularity details on the set of admissible controls and functions  $f, g$ .

## 4.2. Conservative Optimization of Treatment Plans

The expected cost of a candidate treatment plan in [Equation \(3\)](#) cannot be evaluated directly because the structural dynamics governing  $X^{(t_0, x_0, u)}$  are unknown. We therefore learn an approximate dynamics model and use it to compute the expected cost of a treatment plan under the learned dynamics. This model-based objective is ultimately not the quantity of interest: the goal is to find treatment plans that minimize the expected cost under the true dynamics. Directly optimizing the model-based objective can exploit model error and find suboptimal plans under the true dynamics. We address this and derive a tractable upper bound on the true expected cost  $\mathcal{J}(t_0, X^{(t_0, x_0, u)}, u)$  of a plan  $u$ . We propose a consistent estimator for the upper bound and optimize treatment plans by minimizing it. To the best of our knowledge, such a conservative bound – together with a consistent estimator – has not previously been established for the continuous-time setting.

**Estimated Dynamics Model.** We approximate the dynamics from observational data  $\mathcal{D}$  and denote by  $\hat{X}^{(t_0, x_0, u)}$  the model-implied state process under treatment plan  $u$  and initialized at  $\hat{X}_{t_0} = x_0$ . This allows us to evaluate a model-based surrogate cost  $\mathcal{J}(t_0, \hat{X}^{(t_0, x_0, u)}, u)$ . In principle, any identification method can be used, provided the chosen model class is rich enough to contain (or closely approximate) the structural dynamics model in [Equation \(2\)](#). In our experiments, we instantiate the model class with a neural stochastic differential equation (neural SDE; see,

e.g., Kidger (2022)). Specifically, we parameterize drift and diffusion by neural networks  $\mu_\theta : \mathbb{R}^{d_x} \times A \rightarrow \mathbb{R}^{d_x}$  and  $\sigma_\theta : \mathbb{R}^{d_x} \times A \rightarrow \mathbb{R}^{d_x \times d_w}$ , and define  $\hat{X}$  as the strong solution of

$$d\hat{X}_t = \mu_\theta(\hat{X}_t, U_t) dt + \sigma_\theta(\hat{X}_t, U_t) dW_t, \quad (4)$$

where  $W$  is a  $d_w$ -dimensional Brownian motion. To generate the rollout  $\hat{X}^{(t_0, x_0, u)}$ , we set  $U_t = u_t$  and initialize the SDE at  $\hat{X}_{t_0} = x_0$ .

**Decomposition of Model Bias.** To derive a conservative bound on the objective, we first relate the true cost of a treatment plan  $u$  and the estimated cost under the learned model. We decompose the error  $\Delta(t_0, x_0, u) := \mathcal{J}(t_0, X^{(t_0, x_0, u)}, u) - \mathcal{J}(t_0, \hat{X}^{(t_0, x_0, u)}, u)$  over a temporal partition  $t_0 < t_1 < \dots < t_K = t_f$  and express it as a telescoping sum of conditional one-step discrepancies on shorter time intervals. We comment later on further motivation of the decomposition in shorter time intervals.

**Lemma 4.7** (Value Error Telescope). *For an admissible control  $(u : I \rightarrow \mathbb{R}^{d_u}) \in \mathcal{U}_{\text{adm}}$  and initial condition  $x_0$ ,*

$$\Delta(t_0, x_0, u) = \sum_{j=0}^{K-1} \mathbb{E}_{x \sim P_{\hat{X}_{t_j}}} [D_j(x, u)]$$

with one-step discrepancy on  $[t_j, t_{j+1}]$  between true and learned dynamics given by

$$D_j(x, u) = \mathbb{E}_{\hat{x}_{[t_j, t_{j+1}]} \sim P_{\hat{X}_{[t_j, t_{j+1}]}} | \hat{X}_{t_j} = x} [h_j(\hat{x}_{[t_j, t_{j+1}]})] \\ - \mathbb{E}_{x_{[t_j, t_{j+1}]} \sim P_{X_{[t_j, t_{j+1}]}} | X_{t_j} = x} [h_j(x_{[t_j, t_{j+1}]})]$$

and  $h_j$  is the deterministic path functional

$$x_{[t_j, t_{j+1}]} \mapsto \int_{t_j}^{t_{j+1}} f(t, x_s, u_s) ds + \mathcal{J}(t_{j+1}, x_{t_{j+1}}, u)$$

mapping a deterministic path segment  $x_{[t_j, t_{j+1}]}$  to the cumulative cost on the current sub interval  $[t_j, t_{j+1}]$  plus the continuation value at  $t_{j+1}$ .

The lemma extends related results from discrete (Luo et al., 2019) to the continuous-time setting; the detailed proof can be found in Appendix C.1.

With Lemma 4.7 we can upper bound the true costs  $\mathcal{J}(t_0, X^{(t_0, x_0, u)}, u)$  under a candidate control  $u$  via

$$\mathcal{J}(t_0, X^{(t_0, x_0, u)}, u) \leq \mathcal{J}(t_0, \hat{X}^{(t_0, x_0, u)}, u) \\ + \sum_{j=0}^{K-1} \mathbb{E}_{x \sim P_{\hat{X}_{t_j}}} [|D_j(x, u)|].$$

This suggests that a treatment plan with low model-based cost and small accumulated one-step discrepancies will also

have low cost under the true dynamics. The difficulty is that  $D_j(x, u)$  depends on the true conditional law and on the continuation value under the true dynamics. To obtain a data-support-aware bound that depends only on distributional differences between the true and learned dynamics, we upper bound each one-step discrepancy by an integral probability metric (IPM) between the corresponding conditional path laws (cf. the discrete-time argument in (Yu et al., 2020)). For any function class  $\mathcal{G} \subseteq \mathcal{L}^0(\mathbb{R}^{d_x} | [t_j, t_{j+1}], \mathbb{R})$  with  $h_j \in \mathcal{G}$ , the one-step discrepancy satisfies

$$|D_j(y, u)| \leq \text{IPM}_{\mathcal{G}}[P_{X_{[t_j, t_{j+1}]}} | X_{t_j} = y, P_{\hat{X}_{[t_j, t_{j+1}]}} | \hat{X}_{t_j} = y]$$

where  $\text{IPM}_{\mathcal{G}}(P, Q) := \sup_{g \in \mathcal{G}} |\mathbb{E}_P[g] - \mathbb{E}_Q[g]|$  is the integral probability metric generated by  $\mathcal{G}$ . Common choices for  $\mathcal{G}$  in machine learning include the following (see Appendix D for details):

- (i) The total variation distance is induced by  $\mathcal{G}_{TV} = \{f \in \mathcal{L}^0(\mathcal{X}, \mathbb{R}) \mid \sup_{x \in \mathcal{X}} |f(x)| \leq 1\}$ ;
- (ii) Given an RKHS  $(H \subseteq \mathbb{C}^{\mathcal{X}}, \langle \cdot, \cdot \rangle_H, k : \mathcal{X} \times \mathcal{X} \rightarrow \mathbb{C})$ , the IPM for  $\mathcal{G}_H = \{f \in H \mid \|f\|_H \leq 1\}$  is called maximum mean discrepancy (MMD), denoted  $\text{MMD}_k$ ;
- (iii) Given a metric space  $(\mathcal{X}, d)$  ( $\mathcal{A}_{\mathcal{X}} = \mathcal{B}(\mathcal{T}_d)$ ), the IPM for  $\mathcal{G}_W = \{f \in L^0(\mathcal{X}, \mathbb{R}) \cap B(\mathcal{X}, \mathbb{R}) \mid \|f\|_L := \sup_{x \neq y} \frac{|f(x) - f(y)|}{d(x, y)} \leq 1\}$  is called earth mover or Wasserstein or  $L^1$ -distance.

Due to the Lipschitz-regularity assumptions on the structural dynamics model, the evolution over a finite time-horizon and the boundedness of objective functions (Appendix B), we can assume there exists a  $c \in \mathbb{R}_{>0}$  s.t.  $\frac{h_j}{c} \in \mathcal{G}$ , and thus

$$|D_j(y, u)| \leq c \cdot \text{IPM}_{\mathcal{G}}[P_{X_{[t_j, t_{j+1}]}} | X_{t_j} = y, P_{\hat{X}_{[t_j, t_{j+1}]}} | \hat{X}_{t_j} = y].$$

**Conservative Objective.** From this, we can alter our optimization objective to a conservative ‘‘out-of-distribution aware’’ upper-bound objective

$$\min_{u \in \mathcal{U}_{\text{adm}}} \mathbb{E} \left[ \int_{t_0}^{t_f} f(t, \hat{X}_t^{(t_0, x_0, u)}, u_t) dt + g(\hat{X}_{t_f}^{(t_0, x_0, u)}) \right] \quad (5)$$

$$+ \lambda \sum_{j=0}^{K-1} \mathbb{E} \left[ \text{IPM}_{\mathcal{G}}[P_{X_{[t_j, t_{j+1}]}} | X_{t_j} = x_{t_j}, P_{\hat{X}_{[t_j, t_{j+1}]}} | \hat{X}_{t_j} = x_{t_j}] \right]$$

where  $\lambda > 0$  is a hyperparameter controlling the degree of conservatism.

**Signature Kernel-Based Estimator.** As we cannot access the true conditional path distributions, one possibility to describe the MMD between  $P_{X|u, x_0}$  and  $P_{\hat{X}|u, x_0}$  is via the maximum conditional mean discrepancy (MCMD) (Park & Muandet, 2020), through conditional mean embeddings (CME) in a suitable reproducing kernel Hilbert

space (RKHS), The MCMD has the advantage of working purely on RKHS embeddings (e.g., avoid density estimation) and offering a consistent (regularized) kernel-ridge-type estimator (Park et al., 2021) that is tractable purely from observational data (see Appendix D for details). Since  $X$  is a path, the choice of kernel must be defined on path space. A natural choice for the kernel can be constructed via the signature transform, which is a feature map  $\mathcal{S} : C_p(I, \mathbb{R}^d) \rightarrow H_S(\mathbb{R}^d)$  that converts a continuous path  $x \in C_p(\mathbb{R}^d)$  of bounded variation into a graded sequence of iterated integrals

$$\mathcal{S}(x) = \left(1, \mathcal{S}^{(1)}(x), \dots, \mathcal{S}^{(k)}(x), \dots\right) \in \prod_{k=0}^{\infty} (\mathbb{R}^d)^{\otimes k},$$

$$\mathcal{S}^{(k)}(x) = \int_{t_0 < t_1 < \dots < t_k < t_f} dx_{t_1} \otimes \dots \otimes dx_{t_k} \in (\mathbb{R}^d)^{\otimes k}$$

that form an expressive representation of the path in the Hilbert space  $\prod_{k=0}^{\infty} (\mathbb{R}^d)^{\otimes k} =: H_S(\mathbb{R}^d)$  and capture the order and interaction of its increments. An analogy is often drawn to monomials: just as polynomials are dense in  $C(K)$  on compact  $K \subset \mathbb{R}^d$  by Stone–Weierstraß, finite linear combinations of signature coordinates are dense in the continuous functionals on suitable compact sets of paths, so the signature gives a universal feature map for path-valued data. Equipped with the canonical Hilbert space structure on  $H_S(\mathbb{R}^d)$ , the signature feature map induces the signature kernel

$$k_{\text{sig}}(x, y) := \langle \mathcal{S}(x), \mathcal{S}(y) \rangle_{H_S(\mathbb{R}^d)},$$

s.t. the CME of the conditional distributions  $P_{X|U}$ , can be computed via  $\mu_{P_{X|U}} := \mathbb{E}[k_{\text{sig}}(X, \cdot) | U]$ . This establishes the signature kernel MMD  $\text{MMD}_{k_{\text{sig}}}(P_X, P_Y) = \|\mu_{P_X} - \mu_{P_Y}\|_{H_S(\mathbb{R}^d)}$  that we can use for estimating the IPM in our conservative objective. The full formal estimator is given in Appendix C. Instead of explicitly computing higher-order signature features directly, the signature kernel can be more efficiently evaluated by solving a Goursat-PDE, see (Salvi et al., 2021; Cass & Salvi, 2024).

**On the Partition of the Time Interval.** Our results are stated for an arbitrary partition  $t_0 < t_1 < \dots < t_K = t_f$  of the horizon  $I$ . For the objective in Equation (3), one may simply take  $K = 1$  and optimize over the full interval (we do so; details in Section 5). We nonetheless keep the partitioned form because it aligns with standard numerical practice in optimal control. In particular, multi-shooting splits the horizon into shorter intervals and optimizes over the resulting segments, which often improves stability for complex dynamics over long time-horizons, compared to single shooting (Gros & Diehl, 2020). Our formulation supports this through the choice of  $K > 1$ . The same segment-wise viewpoint also connects naturally to offline model-based RL, where long rollouts under a learned model

can amplify error and motivate local control of discrepancies, for instance via adaptive rollout truncation (Koprulu et al., 2025; Zhang et al., 2023).

## 5. Experimental Setup

We evaluate and benchmark our treatment optimization approach on simulated, irregularly sampled longitudinal patient trajectories generated from state-of-the-art pharmacokinetic–pharmacodynamic (PK/PD) models. This is a standard approach in longitudinal treatment-effect estimation and allows us to evaluate ground-truth outcomes under optimized treatment plans.

**Data.** We use the lung cancer tumor growth simulator of Geng et al. (2017), which models the combined effects of chemotherapy and radiotherapy and is widely used for longitudinal treatment-effect estimation (Kacprzyk et al., 2024; Seedat et al., 2022; Hess et al., 2023; Hess & Feuerriegel, 2025). We randomly select between two clinically motivated treatment plans (Curran Jr et al., 2011): sequential therapy (three weeks of weekly chemotherapy followed by three weeks of radiotherapy) and concurrent therapy (bi-weekly joint chemo–radiotherapy). The state and control dimensions are  $d_x = 2$  and  $d_u = 2$  (tumor volume and drug concentration; chemotherapy and radiotherapy dosing). We simulate trajectories over a 60-day horizon and induce irregular sampling by masking 30% of measurements at random.

In addition, we adopt the Covid-19 disease progression model under dexamethasone treatment of Qian et al. (2021), which is an extension of Dai et al. (2021). We consider a single-intervention setting in a 14-day window, where dexamethasone is administered at one of three predefined time points with randomly sampled dosage  $d \in [0, 10]$ . The control is the plasma dexamethasone concentration ( $d_u = 1$ ), and the state comprises viral load, innate immune response, adaptive immune response, and lung-tissue dexamethasone concentration ( $d_x = 4$ ). We simulate trajectories over a 14-day horizon and induce irregular sampling by masking 30% of measurements at random.

**Treatment Optimization Objectives.** We consider a total of three treatment optimization objectives. In the cancer problem, we consider two treatment optimization objectives. The first objective (*absolute target*) minimizes tumor volume at the terminal time  $t_f$  while penalizing treatment intensity to discourage overly aggressive dosing. The second objective (*relative target*) encourages achieving a fixed relative reduction in tumor volume (70%) with respect to the initial volume, again trading off tumor control against treatment intensity. In the Covid-19 problem, we define a desired target trajectory that mirrors the average disease progression and optimize the treatment to track this trajectory

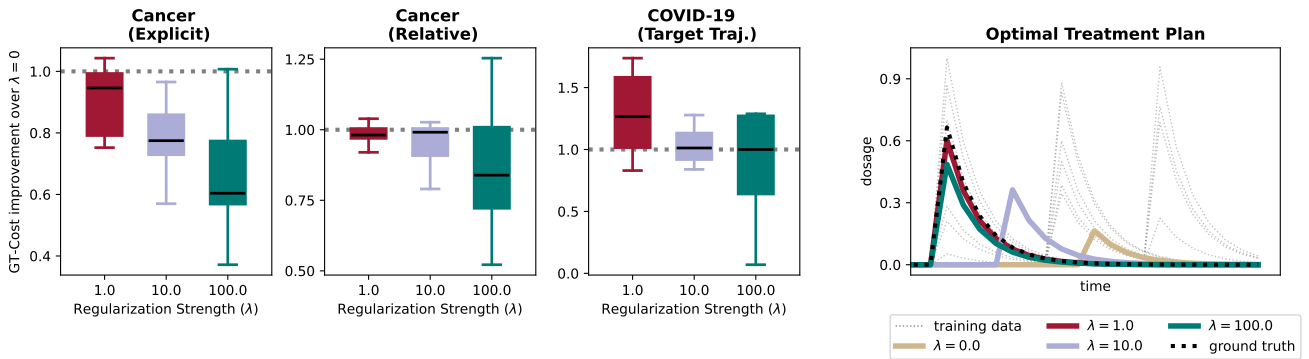


Figure 1. Effect of increasing regularization strength  $\lambda$ . (Left) Improvement of the ground truth costs for  $\lambda = \{1, 10, 100\}$  relative to the ground truth costs with no regularization, i.e.,  $\lambda = 0$  on three optimization problems across 15 different initial conditions (Cancer (Explicit), Cancer (Relative), Covid-19 (Target Trajectory)). Boxplots show medians and interquartile ranges (IQR). Whiskers extend to the farthest point within  $1.5 \times \text{IQR}$  from boxes. (Right) Example of predicted optimal treatment plans for  $\lambda \in \{0, 1, 10, 100\}$  together with treatment plans seen during training and ground truth optimal treatment plan.

Table 1. Benchmarking the optimized treatment plans on all three tasks; Cancer (Explicit), Cancer (Relative) and Covid-19 (Target Trajectory).

(a) Average Spearman correlation between predicted costs and true costs of the candidate treatment plans in the control library. Higher values indicate better results.

Method	Cancer (Explicit)	Cancer (Relative)	Covid-19 (Target Traj.)
TECDE	$0.29 \pm 0.01$	$-0.30 \pm 0.10$	$0.79 \pm 0.34$
INSITE/SINDy	$-0.77 \pm 0.00$	$-0.78 \pm 0.00$	$0.43 \pm 0.35$
<b>Ours (rank)</b>	$0.40 \pm 0.0$	$0.23 \pm 0.02$	$0.51 \pm 0.24$

(b) Average true costs of the optimized treatment plans. For our approach, we use a regularization strength of  $\lambda = 100$ . Lower values indicate better results.

Method	Cancer (Explicit)	Cancer (Relative)	Covid-19 (Target Traj.)
TECDE	$467.26 \pm 726.64$	$280.97 \pm 414.76$	$5.80 \pm 2.55$
INSITE/SINDy	$559.74 \pm 824.42$	$333.77 \pm 490.53$	$7.59 \pm 3.83$
<b>Ours (<math>\lambda = 100</math>)</b>	$242.07 \pm 314.60$	$73.42 \pm 108.34$	$5.61 \pm 3.79$

(target trajectory). We solve each optimization problem for 15 randomly sampled initial conditions. Exact mathematical definitions of all objectives are provided in Appendix E.2.

**Practical Implementation.** Our proposed approach is modular, separating (i) learning a continuous-time dynamics model from observational trajectories and (ii) optimizing a conservative treatment objective under the learned dynamics. While any dynamics identification method whose model class contains the true structural dynamics could be used, we instantiate the dynamics with a neural SDE by parameterizing the drift and diffusion in Equation (2) with neural networks, and train it using an adaptation of the signature-kernel score method of Issa et al. (2023) that conditions on an initial state and control path (details in Appendix E). For treatment optimization, we restrict to a parameterized family of deterministic open-loop controls  $u_\phi : [t_0, t_f] \rightarrow \mathbb{R}^{d_u}$  (see Appendix E.3). In our settings, the parameters  $\phi$  describe the timepoints and dosage values of our treatment (chemo- and radio-therapy for cancer, and Dexamethasone for Covid-19). We then compute optimized plans by gradient-based optimization over  $\phi$ : at each iteration we sample trajectories from the learned neural SDE under  $u_\phi$ , form a Monte-Carlo estimate of the (conservative) objective  $\mathcal{J}(t_0, X^{(t_0, x_0, u)}, u_\phi)$  with numerical integration,

and backpropagate through the solver, corresponding to direct single-shooting approach in optimal control (Hoglund et al., 2023; Gros & Diehl, 2020).

**Baselines.** We benchmark against state-of-the-art continuous-time treatment effect estimators. Specifically, we implement TE-CDE (Seedat et al., 2022) and INSITE (Kacprzyk et al., 2024). TE-CDE is based on neural controlled differential equations and predicts potential outcomes by conditioning on the full observed history of covariates and treatments. INSITE learns an explicit dynamical model via sparse identification of nonlinear dynamics (SINDy) (Brunton et al., 2016a). Implementation details and hyperparameter ranges are reported in Appendix E. To ensure a fair comparison, all baselines are tuned on held-out validation data by selecting hyperparameters that minimize the mean square error of predictions.

Since the baseline methods do not trivially extend to treatment optimization, we evaluate them using a control-library protocol (Seedat et al., 2022; Wang et al., 2025). Concretely, for each optimization problem, we generate a library of 100 candidate control functions by sampling from the same control parameterization used in our optimization procedure. Each baseline then predicts the state trajectory and

the corresponding objective value for every candidate control, and selects the treatment plan with the lowest predicted objective.

## 6. Experimental Results

**Our approach finds better treatment plans compared to baselines.** Table 1 (left) reports Spearman rank correlation between predicted and ground-truth costs on a fixed library of candidate treatment plans. This measures whether a method preserves the cost-induced ordering of candidate plans (i.e., whether plans with low ground-truth cost are also assigned low predicted cost). For our method, we compute predicted costs by simulating the learned neural SDE under each candidate plan. On both cancer tasks, our approach yields the highest rank correlation, indicating a closer match to the ground-truth ordering; on the Covid-19 task, TE-CDE performs best, followed by our approach. Note that this evaluation does not involve optimizing over controls and therefore does not probe model-exploitation effects, since the candidate library remains close to the training distribution. Table 1 (right) reports the ground-truth costs of the optimized treatment plans, evaluated under the true dynamics. Here, our method achieves the lowest average cost across all three tasks.

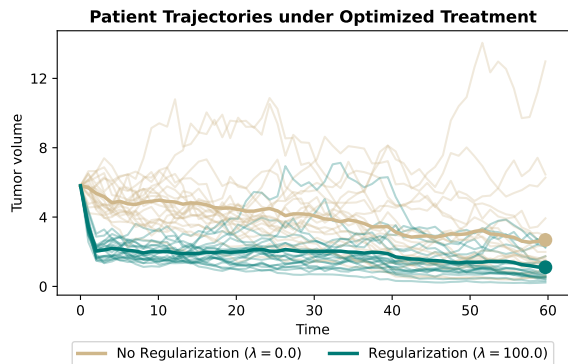


Figure 2. Example patient trajectories under treatment plans optimized with different conservatism levels ( $\lambda$ ). Tumor volume over time for two optimized treatment plans. Shaded regions indicate variability across simulated trajectories, the bold curve denotes the mean trajectory, and the dot marks the mean final tumor volume.

**Increasing regularization strengths  $\lambda$  can improve treatment plan performance.** Figure 1 investigates the effect of the conservative regularization strength  $\lambda$  on treatment optimization. For each test instance, we optimize the control under the learned dynamics for  $\lambda \in \{0, 1, 10, 100\}$  and evaluate the resulting plan using the ground-truth simulator cost  $\mathcal{J}(t_0, X^{(t_0, x_0, u)}, u)$ . We report the relative change in ground-truth cost compared to the unregularized solution

( $\lambda = 0$ ). On both cancer tasks, increasing  $\lambda$  yields a consistent reduction in ground-truth cost, indicating that conservatism mitigates model exploitation during optimization. For the Covid-19 task, we do not observe a clear monotonic trend, but regularization does not degrade performance. A plausible explanation is that the optimized plans remain closer to the training distribution in this task, so distribution-shift effects are less pronounced. As expected, a large  $\lambda$  can eventually dominate the objective and limit further improvements. The left panel of Figure 1 shows an example of the optimized treatment plan in the Covid-19 task for different values of  $\lambda$ ; in this instance, stronger regularization moves the solution closer to the ground-truth optimum. Figure 2 shows the distribution of ground-truth outcome trajectories for a representative patient under the optimized treatment plans with  $\lambda = 0$  and  $\lambda = 100$ . The conservative solution ( $\lambda = 100$ ) achieves a lower mean tumor-volume trajectory and final state, mirroring the cost gains from regularization observed in Figure 1.

## 7. Conclusion

We introduced a conservative continuous-time framework for treatment optimization from irregularly sampled patient trajectories. We propose to model the patient dynamics as a controlled stochastic differential equation where the treatment is a continuous-time control input. To avoid model exploitation during treatment optimization, we derived a conservative objective that augments the model-based cost with a consistent signature-based MMD regularizer, which penalizes plans whose learned model rollout distribution deviates from the observational trajectory distribution via conditional MMD on path space. Experiments on pharmacokinetic–pharmacodynamic simulations show that our conservative objective can improve robustness and lead to better treatment plans under the true dynamics compared to the unregularized setting and baseline approaches.

## Impact Statement

This paper develops technical methodology for conservative, continuous-time treatment optimization from irregularly sampled observational trajectories, with the goal of improving the reliability of planning under learned dynamics; if translated responsibly, such tools could support better decision-making in high-stakes settings (e.g., proposing candidate dosing plans for further expert review, simulation, and prospective study) and may also benefit other domains that require robust control from logged data. At the same time, there are meaningful risks: observational data can reflect selection effects, unmeasured confounding, missingness, and societal or clinical biases, and optimizing over learned models can still produce misleading or harmful recommendations if deployed without rigorous validation, appropriate

constraints, and human oversight; additionally, clinical and behavioral data raise privacy and security concerns. Our work is primarily methodological and does not constitute a deployable medical device or clinical guidance; rather, it aims to advance broadly applicable machine learning foundations for reliable offline optimization, while explicitly emphasizing the importance of safety, uncertainty, and out-of-distribution robustness in any real-world use, particularly in healthcare.

## Acknowledgements

We thank Junhyung Park for his time and for helpful discussions about the paper and the MCMD estimator. We thank Cristopher Salvi for answering questions about the Signature Scores for neural SDE training. We thank Emilio Ferrucci for answering questions about causal identifiability, stochastic control, rough path theory, and for sharing useful pointers to the related literature. This work has been supported by the German Federal Ministry of Education and Research (Grant: 01IS24082).

## References

- Brunton, S. L., Proctor, J. L., and Kutz, J. N. Discovering governing equations from data by sparse identification of nonlinear dynamical systems. *Proceedings of the national academy of sciences*, 113(15):3932–3937, 2016a.
- Brunton, S. L., Proctor, J. L., and Kutz, J. N. Sparse Identification of Nonlinear Dynamics with Control (SINDYc)\*\*SLB acknowledges support from the U.S. Air Force Center of Excellence on Nature Inspired Flight Technologies and Ideas (FA9550-14-1-0398). JLP thanks Bill and Melinda Gates for their active support of the Institute of Disease Modeling and their sponsorship through the Global Good Fund. JNK acknowledges support from the U.S. Air Force Office of Scientific Research (FA9550-09-0174). *IFAC-PapersOnLine*, 49(18):710–715, 2016b. ISSN 24058963. doi: 10.1016/j.ifacol.2016.10.249. URL <https://linkinghub.elsevier.com/retrieve/pii/S2405896316318298>.
- Cass, T. and Salvi, C. Lecture notes on rough paths and applications to machine learning. *arXiv preprint arXiv:2404.06583*, 2024.
- Chakraborty, B. and Murphy, S. A. Dynamic treatment regimes. *Annual review of statistics and its application*, 1(1):447–464, 2014.
- Curran Jr, W. J., Paulus, R., Langer, C. J., Komaki, R., Lee, J. S., Hauser, S., Movsas, B., Wasserman, T., Rosenthal, S. A., Gore, E., et al. Sequential vs concurrent chemoradiation for stage iii non-small cell lung cancer: randomized phase iii trial rtog 9410. *Journal of the National Cancer Institute*, 103(19):1452–1460, 2011.
- Dai, W., Rao, R., Sher, A., Tania, N., Musante, C. J., and Allen, R. A prototype qsp model of the immune response to sars-cov-2 for community development. *CPT: pharmacometrics & systems pharmacology*, 10(1):18–29, 2021.
- De Brouwer, E., Gonzalez, J., and Hyland, S. Predicting the impact of treatments over time with uncertainty aware neural differential equations. In *International Conference on Artificial Intelligence and Statistics*, pp. 4705–4722. PMLR, 2022.
- D’Amour, A., Ding, P., Feller, A., Lei, L., and Sekhon, J. Overlap in observational studies with high-dimensional covariates. *Journal of Econometrics*, 221(2):644–654, 2021.
- Geng, C., Paganetti, H., and Grassberger, C. Prediction of treatment response for combined chemo-and radiation therapy for non-small cell lung cancer patients using a bio-mathematical model. *Scientific reports*, 7(1):13542, 2017.
- Gros, S. and Diehl, M. Numerical optimal control (draft), 2020.
- Hess, K. and Feuerriegel, S. Stabilized neural prediction of potential outcomes in continuous time. In *The Thirteenth International Conference on Learning Representations*, 2025. URL <https://openreview.net/forum?id=aN57tSd5Us>.
- Hess, K., Melnychuk, V., Frauen, D., and Feuerriegel, S. Bayesian neural controlled differential equations for treatment effect estimation. *arXiv preprint arXiv:2310.17463*, 2023.
- Hızlı, Ç., John, S., Juuti, A. T., Saarinen, T. T., Pietiläinen, K. H., and Marttinen, P. Causal modeling of policy interventions from treatment-outcome sequences. In *International Conference on Machine Learning*, pp. 13050–13084. PMLR, 2023.
- Hoglund, M., Ferrucci, E., Hernández, C., Gonzalez, A. M., Salvi, C., Sánchez-Betancourt, L., and Zhang, Y. A neural rde approach for continuous-time non-markovian stochastic control problems. *arXiv preprint arXiv:2306.14258*, 2023.
- Imbens, G. W. and Rubin, D. B. *Causal inference in statistics, social, and biomedical sciences*. Cambridge university press, 2015.
- Issa, Z., Horvath, B., Lemercier, M., and Salvi, C. Non-adversarial training of neural sdes with signature kernel scores. *Advances in Neural Information Processing Systems*, 36:11102–11126, 2023.

- Kacprzyk, K., Holt, S., Berrevoets, J., Qian, Z., and van der Schaar, M. Ode discovery for longitudinal heterogeneous treatment effects inference. *arXiv preprint arXiv:2403.10766*, 2024.
- Kidambi, R., Rajeswaran, A., Netrapalli, P., and Joachims, T. Morel: Model-based offline reinforcement learning. *Advances in neural information processing systems*, 33: 21810–21823, 2020.
- Kidger, P. On neural differential equations, 2022. URL <https://arxiv.org/abs/2202.02435>.
- Koprulu, C., Djeumou, F., and ufuk topcu. Neural stochastic differential equations for uncertainty-aware offline RL. In *The Thirteenth International Conference on Learning Representations*, 2025. URL <https://openreview.net/forum?id=hxUMQ4fic3>.
- Li, Z., Chen, J., Laber, E., Liu, F., and Baumgartner, R. Optimal treatment regimes: a review and empirical comparison. *International Statistical Review*, 91(3):427–463, 2023.
- Lok, J. J. Statistical modeling of causal effects in continuous time. *The Annals of Statistics*, 36(3):1464–1507, June 2008. doi: 10.1214/009053607000000820. URL <https://doi.org/10.1214/009053607000000820>.
- Luo, Y., Xu, H., Li, Y., Tian, Y., Darrell, T., and Ma, T. Algorithmic framework for model-based deep reinforcement learning with theoretical guarantees. In *International Conference on Learning Representations (ICLR)*, 2019. arXiv:1807.03858.
- Murphy, S. A. Optimal dynamic treatment regimes. *Journal of the Royal Statistical Society Series B: Statistical Methodology*, 65(2):331–355, 2003.
- Park, J. and Muandet, K. A measure-theoretic approach to kernel conditional mean embeddings. In *Advances in Neural Information Processing Systems*, volume 33, pp. 16665–16677, 2020. doi: 10.5555/3495724.3497508. URL <https://proceedings.neurips.cc/paper/2020/hash/f340f1b1f65b6df5b5e3f94d95b11daf-Abstract.html>.
- Park, J., Shalit, U., Schölkopf, B., and Muandet, K. Conditional distributional treatment effect with kernel conditional mean embeddings and u-statistic regression. In Meila, M. and Zhang, T. (eds.), *Proceedings of the 38th International Conference on Machine Learning*, volume 139 of *Proceedings of Machine Learning Research*, pp. 8401–8412. PMLR, July 2021. URL <https://proceedings.mlr.press/v139/park21c.html>.
- Pham, H. *Continuous-time Stochastic Control and Optimization with Financial Applications*, volume 61 of *Stochastic Modelling and Applied Probability*. Springer, Berlin, Heidelberg, 2009. ISBN 978-3-540-89499-5 978-3-540-89500-8. doi: 10.1007/978-3-540-89500-8. URL <https://link.springer.com/10.1007/978-3-540-89500-8>.
- Qian, Z., Zame, W., Fleuren, L., Elbers, P., and van der Schaar, M. Integrating expert odes into neural odes: pharmacology and disease progression. *Advances in Neural Information Processing Systems*, 34:11364–11383, 2021.
- Robins, J. M. Optimal structural nested models for optimal sequential decisions. In *Proceedings of the Second Seattle Symposium in Biostatistics: analysis of correlated data*, pp. 189–326. Springer, 2004.
- Salvi, C., Cass, T., Foster, J., Lyons, T., and Yang, W. The Signature Kernel is the solution of a Goursat PDE. *SIAM Journal on Mathematics of Data Science*, 3:873–899, January 2021. ISSN 2577-0187. doi: 10.1137/20M1366794. URL <http://arxiv.org/abs/2006.14794>. arXiv:2006.14794 [math].
- Schulam, P. and Saria, S. Reliable decision support using counterfactual models. *Advances in neural information processing systems*, 30, 2017.
- Seedat, N., Imrie, F., Bellot, A., Qian, Z., and van der Schaar, M. Continuous-time modeling of counterfactual outcomes using neural controlled differential equations. *arXiv preprint arXiv:2206.08311*, 2022.
- Sun, J. and Crawford, F. W. Causal identification for continuous-time stochastic processes. *arXiv preprint arXiv:2211.15934*, 2022.
- Tsirtsis, S. and Rodriguez, M. Finding counterfactually optimal action sequences in continuous state spaces. *Advances in Neural Information Processing Systems*, 36: 3220–3247, 2023.
- Vanderschueren, T., Curth, A., Verbeke, W., and Van Der Schaar, M. Accounting for informative sampling when learning to forecast treatment outcomes over time. In *International Conference on Machine Learning*, pp. 34855–34874. PMLR, 2023.
- Wang, X., Lyu, S., Luo, C., Zhou, X., and Chen, H. Variational counterfactual intervention planning to achieve target outcomes. In *Forty-second International Conference on Machine Learning*, 2025. URL <https://openreview.net/forum?id=ggvHPOXLGH>.
- Xu, Y. and Zhang, Z. Modeling and optimizing dynamic treatment regimens in continuous time. In *Statistics in Precision Health: Theory, Methods and Applications*, pp. 513–535. Springer, 2024.

- Ying, A. Causal identification for complex functional longitudinal studies. In *The Thirteenth International Conference on Learning Representations*, 2025. URL <https://openreview.net/forum?id=96beVMeHh9>.
- Yu, T., Thomas, G., Yu, L., Ermon, S., Zou, J. Y., Levine, S., Finn, C., and Ma, T. Mopo: Model-based offline policy optimization. *Advances in Neural Information Processing Systems*, 33:14129–14142, 2020.
- Yu, T., Kumar, A., Rafailov, R., Rajeswaran, A., Levine, S., and Finn, C. Combo: Conservative offline model-based policy optimization. *Advances in neural information processing systems*, 34:28954–28967, 2021.
- Zhang, J., Lyu, J., Ma, X., Yan, J., Yang, J., Wan, L., and Li, X. Uncertainty-driven trajectory truncation for data augmentation in offline reinforcement learning. *arXiv preprint arXiv:2304.04660*, 2023.
- Zhou, Y., Qi, Z., Shi, C., and Li, L. Optimizing pessimism in dynamic treatment regimes: A bayesian learning approach. In *International Conference on Artificial Intelligence and Statistics*, pp. 6704–6721. PMLR, 2023.

Table 2. Summary of notation

Symbol	Meaning
$I$	$I := [t_s, t_f]$ , the considered finite time horizon
$N$	the number of training samples
$\mathcal{D}$	the dataset $\mathcal{D} := \{(z^{(i)}, y^{(i)}, u^{(i)})\}_{i \in [N]}$
$d_z$	dimension of the stochastic covariate process $Z : \Omega \times I \rightarrow \mathbb{R}^{d_z}$
$d_y$	dimension of the stochastic outcome process $Y : \Omega \times I \rightarrow \mathbb{R}^{d_y}$
$d_u$	dimension of the stochastic treatment process $U : \Omega \times I \rightarrow \mathbb{R}^{d_u}$
$d_x$	$d_x = d_z + d_y$ dimension of $X = (Z, Y)^\top$
$\mathcal{M}_1(\Omega, \mathcal{A})$	the set of probability measures on measurable space $(\Omega, \mathcal{A})$
$\mathcal{Y}^{\mathcal{X}}$	the set of all functions $\text{Funct}(\mathcal{X}, \mathcal{Y}) = \{f : \mathcal{X} \rightarrow \mathcal{Y}\}$
$\mathcal{L}^0((\mathcal{X}, \mathcal{A}_{\mathcal{X}}), (\mathcal{Y}, \mathcal{A}_{\mathcal{Y}}))$	the $\mathcal{A}_{\mathcal{X}} - \mathcal{A}_{\mathcal{Y}}$ measurable functions $f : \mathcal{X} \rightarrow \mathcal{Y}$

## A. Summary of Notation

A summary of notation is provided in Table 2. We write  $u$  for a sample of the stochastic process  $U$ .

## B. On Identifiability for Continuous-Time Treatment Effects

In order to render the stochastic control problem from Equation (1) computationally tractable, we reformulated it as Equation (3). In this section we (i) give regularity assumptions on the controlled dynamics that guarantee existence and uniqueness of the resulting state trajectory, (ii) specify the assumptions for Equation (1) to be identifiable, and (iii) narrow down the class of admissible treatment processes for the control problem to be well-defined. Concretely, we model the patient state by a controlled SDE with measurable drift- and diffusion functions, satisfying the standard conditions (e.g., uniform Lipschitz continuity in the state, plus suitable integrability of the control) so that, for any initial condition  $(t_0, x_0)$  and any admissible control  $u$ , the SDE admits a unique strong solution  $X^{t_0, x_0, u}$  with finite objective.

**Structural Dynamics Model.** Let  $I = [t_s, t_f]$ , let  $(\Omega, \mathcal{F}, \mathbb{F}, P)$  be a complete filtered probability space with filtration  $\mathbb{F} = (\mathcal{F}_t)_{t \in I}$  satisfying the usual conditions,  $W = (W_t)_{t \in I}$  a  $\mathbb{R}^{d_w}$ -valued Wiener process adapted to  $\mathbb{F}$ ,  $U = (U_t)_{t \in I}$  the progressively  $\mathbb{F}$ -measurable control-process taking values in  $A \subseteq \mathbb{R}^{d_u}$  and

$$\mu : \mathbb{R}^{d_x} \times A \rightarrow \mathbb{R}^{d_x}, \quad \sigma : \mathbb{R}^{d_x} \times A \rightarrow \mathbb{R}^{d_x \times d_w}, \quad (6)$$

the measurable drift- and diffusion functions of the controlled SDE

$$dX_t = \mu(X_t, U_t) dt + \sigma(X_t, U_t) dW_t, \quad t \in I. \quad (7)$$

Assuming

- (i) uniform Lipschitz condition in the state, uniformly over treatments, meaning there exists  $K \geq 0$  such that for all  $x, y \in \mathbb{R}^{d_x}$  and all  $u \in A$ ,

$$\|\mu(x, u) - \mu(y, u)\| + \|\sigma(x, u) - \sigma(y, u)\| \leq K\|x - y\|.$$

- (ii) the set of control processes are restricted such that

$$\mathbb{E} \left[ \int_{t_0}^{t_f} \|\mu(0, u_t)\|^2 + \|\sigma(0, u_t)\|^2 dt \right] < \infty$$

the controlled SDE Equation (7) admits a unique strong solution for every initial condition  $(t_0, x_0) \in I \times \mathbb{R}^{d_x}$ , for any progressively  $\mathbb{F}$ -measurable control process  $U$ , which we denote by  $X^{(t_0, x_0, U)} = (X_t^{(t_0, x_0, U)})_{t \in I}$ . For more details see Pham (2009).

**The Class of Admissible Treatments.** Assuming a controlled SDE  $(\mu, \sigma, I)$  as in Equation (7) and measurable functions  $f : I \times \mathbb{R}^{d_x} \times A \rightarrow \mathbb{R}$  and  $g : \mathbb{R}^{d_x} \rightarrow \mathbb{R}$  s.t.

- (i)  $g$  is lower-bounded
- (ii)  $\exists C > 0 : |g(x)| \leq C(1 + |x|^2) \quad \forall x \in \mathbb{R}^n$

the set of admissible controls for  $(t_0, x_0) \in I \times \mathbb{R}^{d_x}$ ,

$$\mathcal{U}_{\text{adm}} := \mathcal{U}_{(t_0, x_0)}^f := \left\{ u \mid \mathbb{E} \left[ \int_{t_0}^{t_f} |f(s, X_s^{(t_0, x_0, u)}, u_s)| ds \right] < \infty \right\} \neq \emptyset$$

is non-empty, making the SDE-governed control problem

$$v(t_0, x_0) = \arg \inf u \in \mathcal{U}_{\text{adm}} \mathcal{J}(t_0, x_0, u), \quad \mathcal{J}(t_0, x_0, u) = \mathbb{E} \left[ \int_{t_0}^{t_f} f(s, X_s^{(t_0, x_0, u)}, u_s) ds + g \left( X_{t_f}^{(t_0, x_0, u)} \right) \right]$$

well-defined, where  $\mathcal{J}(t_0, x_0, \alpha)$  is the cost function and  $v(t_0, x_0)$  the associated value function.

## C. Details on Our Proposed Approach

### C.1. Proof of the telescope lemma

In this subsection, we prove Lemma 4.7, wlog assuming  $I = [0, 1]$  for notational convenience. Note:

*Remark C.1.* Given an admissible  $u \in \mathcal{U}$  we have by the path-wise uniqueness of the flow of the SDE for  $X$ , due to the Markovian structure of the SDE:

$$X_t^{(t_0, x_0, u)} = X_t^{(\tau, X_\tau^{(t_0, x_0, u)}, u)}, \quad t \geq \tau$$

For any stopping time  $\tau$  valued in  $[t_0, 1]$ . Hence we obtain:

$$\mathcal{J}(t_0, x_0, u) = \mathbb{E} \left[ \int_{t_0}^\tau f(s, X_s^{(t_0, x_0, u)}, u_s) ds + \int_\tau^1 f(s, X_s^{(t_0, x_0, u)}, u_s) ds + g(X_1^{(t_0, x_0, u)}) \right] \quad (8)$$

$$\stackrel{(*)}{=} \mathbb{E} \left[ \mathbb{E} \left[ \int_{t_0}^\tau f(s, X_s^{(t_0, x_0, u)}, u_s) ds + \int_\tau^1 f(s, X_s^{(t_0, x_0, u)}, u_s) ds + g(X_1^{(t_0, x_0, u)}) \mid \mathcal{F}_\tau \right] \right] \quad (9)$$

$$\stackrel{(**)}{=} \mathbb{E} \left[ \int_{t_0}^\tau f(s, X_s^{(t_0, x_0, u)}, u_s) ds + \mathbb{E} \left[ \int_\tau^1 f(s, X_s^{(t_0, x_0, u)}, u_s) ds + g(X_1^{(t_0, x_0, u)}) \mid \mathcal{F}_\tau \right] \right] \quad (10)$$

where in  $(*)$  we used the tower property of the conditional expectation and in  $(**)$  we used that  $\tau$  a stopping time making  $\int_{t_0}^\tau f(s, X_s^{(t_0, x_0, u)}, u_s) ds$   $\mathcal{F}_\tau$  measurable. Moreover, by shifting control and Brownian motion by  $-\tau$ , in the underlying controlled SDE, we obtain:

$$\mathbb{E} \left[ \int_\tau^1 f(s, X_s^{(t_0, x_0, u)}, u_s) ds + g(X_1^{(t_0, x_0, u)}) \mid \mathcal{F}_\tau \right] = \mathcal{J}(\tau, X_\tau^{(t_0, x_0, u)}, u) \quad P - \text{a.s.}$$

such that

$$\mathcal{J}(t_0, x_0, u) = \mathbb{E} \left[ \int_{t_0}^\tau f(s, X_s^{(t_0, x_0, u)}, u_s) ds + \mathcal{J}(\tau, X_\tau^{(t_0, x_0, u)}, u) \right]$$

*Proof.* For  $j \in \{0, \dots, K-1\}$ , define the stochastic process  $\tilde{X}^{(j)}$  that evolves up to time  $t_j$  according to (estimated) SDE governed by  $\mu_\theta, \sigma_\theta$  and starting from  $t_j$  according to the true SDE with  $\mu, \sigma$ , meaning  $\tilde{X}^{(i)} = (\tilde{X}_s^{(i)})_{s \in I}$  satisfies

$$\tilde{X}_{[0, t_j]}^{(j)} = \text{solution of} \quad x_0 + \int_0^{t_j} \mu_\theta(\tilde{X}_s^{(j)}, u_s) ds + \int_0^{t_j} \sigma_\theta(\tilde{X}_s^{(j)}) dW_s, \quad (11)$$

$$\tilde{X}_{[t_j, 1]}^{(j)} = \text{solution to} \quad \tilde{X}_{t_j}^{(j)} + \int_{t_j}^1 \mu(\tilde{X}_s^{(j)}, u_s) ds + \int_{t_j}^1 \sigma(\tilde{X}_s^{(j)}) dW_s. \quad (12)$$

Note that  $\tilde{X}^{(0)} := X := X^{(0,x_0,u)}$ ,  $\tilde{X}^{(N)} = \hat{X} = \hat{X}^{(0,x_0,u)}$ . Then for a stopping time  $\tau$ , we can therefore define

$$\tilde{\mathcal{J}}^{(j)} := \mathcal{J}(0, \tilde{X}^{(j)}, u) = \mathbb{E} \left[ \int_0^\tau f(\tilde{X}_s^{(j)}, u) ds + \mathcal{J}(\tau, \tilde{X}_\tau^{(j)}, u) \right]$$

By a "telescoping-sum" argument, we can write

$$\mathcal{J}(0, X^{(0,x_0,u)}, u) - \mathcal{J}(0, \hat{X}^{(0,x_0,u)}, u) = \tilde{\mathcal{J}}^{(0)} - \tilde{\mathcal{J}}^{(N)} = \sum_{j=0}^{N-1} (\tilde{\mathcal{J}}^{(j)} - \tilde{\mathcal{J}}^{(j+1)}).$$

With the choice  $\tau = t_j$ , we can write

$$\begin{aligned} \tilde{\mathcal{J}}^{(j)} &= \mathbb{E} \left[ \int_0^{t_j} f(s, \tilde{X}_s^{(j)}, u_s) ds + \mathbb{E} \left[ \int_{t_j}^1 f(s, \tilde{X}_s^{(j)}, u_s) ds + g(\tilde{X}_1^{(j)}) \mid \tilde{\mathcal{F}}_{t_j}^{(j)} \right] \right] \\ &= \mathbb{E} \left[ \int_0^{t_j} f(s, \tilde{X}_s^{(j)}, u_s) ds + \mathbb{E} \left[ \int_{t_j}^{t_{j+1}} f(s, \tilde{X}_s^{(j)}, u_s) ds + \underbrace{\mathbb{E} \left[ \int_{t_{j+1}}^1 f(s, \tilde{X}_s^{(j)}, u_s) ds + g(\tilde{X}_1^{(j)}) \mid \tilde{\mathcal{F}}_{t_{j+1}}^{(j)} \right]}_{\stackrel{\text{a.s.}}{=} \tilde{\mathcal{J}}(t_{j+1}, \tilde{X}_{t_{j+1}}^{(j)}, u)} \mid \tilde{\mathcal{F}}_{t_j}^{(j)} \right] \right] \end{aligned}$$

where  $\mathcal{F}_t^{(j)} = \sigma(X_s^{(j)} \mid s \leq t)$ . Similarly

$$\tilde{\mathcal{J}}^{(j+1)} = \mathbb{E} \left[ \int_0^{t_j} f(s, \tilde{X}_s^{(j+1)}, u_s) ds + \mathbb{E} \left[ \int_{t_j}^{t_{j+1}} f(\tilde{X}_s^{(j+1)}, u_s) ds + \underbrace{\mathbb{E} \left[ \int_{t_{j+1}}^1 f(\tilde{X}_s^{(j+1)}, u_s) ds + g(\tilde{X}_1^{(j+1)}) \mid \tilde{\mathcal{F}}_{t_{j+1}}^{(j+1)} \right]}_{\stackrel{\text{a.s.}}{=} \mathcal{J}(t_{j+1}, \tilde{X}_{t_{j+1}}^{(j+1)}, u)} \mid \tilde{\mathcal{F}}_{t_j}^{(j+1)} \right] \right]$$

Then, as  $\tilde{X}_s^{(j)} = \tilde{X}_s^{(j+1)} \forall s \leq t_j$ , we have  $\tilde{\mathcal{F}}_{t_j}^{(j)} = \tilde{\mathcal{F}}_{t_j}^{(j+1)}$  from which we can write

$$\begin{aligned} &\tilde{\mathcal{J}}^{(j)} - \tilde{\mathcal{J}}^{(j+1)} \\ &= \mathbb{E} \left[ \mathbb{E} \left[ \left( \int_{t_j}^{t_{j+1}} f(s, \tilde{X}_s^{(j)}, u_s) ds + \mathcal{J}(t_{j+1}, \tilde{X}_{t_{j+1}}^{(j)}, u) \right) - \left( \int_{t_j}^{t_{j+1}} f(s, \tilde{X}_s^{(j+1)}, u_s) ds + \mathcal{J}(t_{j+1}, \tilde{X}_{t_{j+1}}^{(j+1)}, u) \right) \mid \tilde{\mathcal{F}}_{t_j}^{(j)} \right] \right] \\ &\stackrel{(a)}{=} \mathbb{E} \left[ \int_{t_j}^{t_{j+1}} \left( h_j(\tilde{X}_{[t_j, t_{j+1}]}^{(j)}(\omega')) - h_j(\tilde{X}_{[t_j, t_{j+1}]}^{(j+1)}(\omega')) \right) dP^{(t_j)}(\omega, d\omega') \right] \\ &\stackrel{(b)}{=} \mathbb{E}_{y \sim P_{\tilde{\mathcal{X}}_{t_j}^{(j)}}} \left[ \underbrace{\mathbb{E}_{P_{\tilde{\mathcal{X}}_{[t_j, t_{j+1}]}} \mid \tilde{\mathcal{X}}_{t_j} = y} [F_j(\tilde{x}_{[t_j, t_{j+1}]})] - \mathbb{E}_{P_{X_{[t_j, t_{j+1}]}} \mid X_{t_j} = y} [F_j(x_{[t_j, t_{j+1}]})]}_{D_j(y, u)} \right] \end{aligned}$$

where in (a) we inserted the deterministic function  $h_j$  given by

$$(\gamma : [t_j, t_{j+1}] \mapsto \mathbb{R}^n) \longrightarrow \int_{t_j}^{t_{j+1}} f(s, \gamma_s, u_s) ds + \mathcal{J}(t_{j+1}, X^{(t_j, \gamma_{t_{j+1}}, u)}, u)$$

(note: the RHS is a random variable) and in (b) we used a path notation for the push-forward measure. Note the dependence of  $h_j$  on  $u_{[t_j, t_{j+1}]}$ , thus the subscript  $j$ . Altogether we therefore obtain

$$\mathcal{J} - \hat{\mathcal{J}} = \sum_{j=0}^{N-1} \mathbb{E}_{y \sim P_{\tilde{\mathcal{X}}_{t_j}^{(j)}}} \left[ \mathbb{E}_{P_{\tilde{\mathcal{X}}_{[t_j, t_{j+1}]}} \mid \tilde{\mathcal{X}}_{t_j} = y} [h_j(\tilde{x}_{[t_j, t_{j+1}]})] - \mathbb{E}_{P_{X_{[t_j, t_{j+1}]}} \mid X_{t_j} = y} [h_j(x_{[t_j, t_{j+1}]})] \right].$$

□

## C.2. Signature Transform and MCMD Estimator

**The Signature Kernel on Path Space.** A suitable tool for learning from streamed data is the signature transform, a feature map  $\mathcal{S} : C_p(I, \mathbb{R}^d) \rightarrow H_S(\mathbb{R}^d)$  that converts a data stream (a continuous path  $x \in C_p(\mathbb{R}^d)$  of bounded variation) into a graded sequence of iterated integrals

$$\mathcal{S}(x) = \left(1, \mathcal{S}^{(1)}(x), \dots, \mathcal{S}^{(k)}(x), \dots\right) \in \prod_{k=0}^{\infty} (\mathbb{R}^d)^{\otimes k},$$

$$\mathcal{S}^{(k)}(x) = \int_{t_0 < t_1 < \dots < t_k < t_f} dx_{t_1} \otimes \dots \otimes dx_{t_k} \in (\mathbb{R}^d)^{\otimes k}$$

that form an expressive representation of the path in the Hilbert space  $\prod_{k=0}^{\infty} (\mathbb{R}^d)^{\otimes k} =: H_S(\mathbb{R}^d)$  and capture the order and interaction of its increments. An analogy is often drawn to monomials: just as polynomials are dense in  $C(K)$  on compact  $K \subset \mathbb{R}^d$  by Stone–Weierstraß, finite linear combinations of signature coordinates are dense in the continuous functionals on suitable compact sets of paths, so the signature gives a universal feature map for path-valued data. Equipped with the canonical Hilbert space structure on  $H_S(\mathbb{R}^d)$ , the signature feature map induces the signature kernel

$$k_{\text{sig}}(x, y) := \langle \mathcal{S}(x), \mathcal{S}(y) \rangle_{H_S(\mathbb{R}^d)},$$

s.t. laws on path-space can be embedded by the kernel mean map  $\mu_{P_X} := \mathbb{E}[k_{\text{sig}}(X, \cdot)]$  (resp. the conditional mean embedding  $\mu_{P_{X|U}} := \mathbb{E}[k_{\text{sig}}(X, \cdot) | U]$ ), establishing the signature kernel MMD  $\text{MMD}_{k_{\text{sig}}}(P_X, P_Y) = \|\mu_{P_X} - \mu_{P_Y}\|_{H_S(\mathbb{R}^d)}$  that we can leverage to for our model uncertainty regularization.

**Signature-Kernel MCMD Regularizer.** Given distributions  $P_{X,U,X_0}, P_{\hat{X},U,X_0}$  with samples  $\{x^{(i)}, u^{(i)}, x_0^{(i)}\}_{i \in [N]}$ ,  $\{\hat{x}^{(i)}, u^{(i)}, x_0^{(i)}\}_{i \in [N]}$ . Then, for fixed but arbitrary  $x_0 \in \mathbb{R}^n, u \in \mathcal{U}_{adm}$  we have the plug-in estimate for the square of the MCMD function,

$$\begin{aligned} & \hat{M}^2(P_{X|X_0=x_0, U=u}, P_{\hat{X}|X_0=x_0, U=u})(x_0, u) \\ &= k_{X,U}^T(x_0, u) W_{X_0,U} K_X W_{X_0,U}^\top k_{X_0,U}(x_0, u) - 2k_{X_0,U}(x_0, u) W_{X_0,U} K_{X,\hat{X}} W_{X_0,U}^\top k_{X_0,U}(x_0, u) \\ & \quad + k_{X_0,U}^\top(x_0, u) W_{X_0,U} K_{\hat{X}} W_{X_0,U}^\top k_{X_0,U}(x_0, u) \end{aligned}$$

where  $(K_X)_{ij} = k_{\text{sig}}(x^{(i)}, x^{(j)})$ ,  $(K_{\hat{X}})_{ij} = k_{\text{sig}}(\hat{x}^{(i)}, \hat{x}^{(j)})$ ,  $(K_{X,\hat{X}})_{ij} = k_{\text{sig}}(x^{(i)}, \hat{x}^{(j)})$ ,  $(K_{X_0,U})_{ij} = k_{X_0,U}((x_0^{(i)}, u^{(i)}), (x_0^{(j)}, u^{(j)}))$ ,  $W_{X_0,U} = (K_{X_0,U} + n\lambda I_n)^{-1}$ ,  $(k_{X_0,U}(x_0, u))_i = k_{X_0,U}((x_0^{(i)}, u^{(i)}), (x_0, u))$ . Here  $(\mathcal{H}_0 \otimes \mathcal{H}_U, k_{X_0,U})$  is the tensor product of  $(\mathcal{H}_0, k_{X_0})$  the RKHS with  $k_{X_0}$  the rbf and RKHS  $(\mathcal{H}_U, k_U)$ ,  $k_U = k_{\text{sig}}$ , together with the reproducing kernel

$$k_{X_0,U} = k_{X_0} \otimes k_{\text{sig}}$$

Thus  $k_{X_0,U}((x_0^{(i)}, u^{(i)}), (x_0, u)) = k_{X_0}(x^{(i)}, x_0) k_{\text{sig}}(u^{(i)}, u)$ .

## D. Integral probability metrics

To quantify the distance between two probability distributions, a widely used approach is in terms of integral probability metrics (IPM):

**Definition D.1** (Integral probability metric (IPM)). Let  $(\mathcal{X}, \mathcal{A}_{\mathcal{X}})$  be a measurable space,  $P, Q \in \mathcal{M}^1(\mathcal{X}, \mathcal{A}_{\mathcal{X}})$  and  $F \subseteq \mathcal{L}^0(\mathcal{X}, \mathbb{R}) \cap B(\mathcal{X}, \mathbb{R})$  a class of measurable and bounded test functions. The integral probability metric (IPM) generated by  $F$  is

$$\text{IPM}[F, P, Q] := \sup_{f \in F} |\mathbb{E}_P[f] - \mathbb{E}_Q[f]|$$

*Remark D.2.* For the choice of  $F$ , we have the following tradeoff:

- (i) rich enough s.t.  $\text{IPM}[F, P, Q] = 0 \Leftrightarrow P = Q$

(ii) not too large to estimate  $\text{IPM}[F, P, Q]$  quickly

*Example D.3.* Notable function classes, used in machine learning:

- (i) For  $F_{TV} = \{f \in \mathcal{L}^0(\mathcal{X}, \mathbb{R}) \mid \sup_{x \in \mathcal{X}} |f(x)| \leq 1\}$ ,  $\text{IPM}[F, P, Q] =: \|P - Q\|_{TV}$  is called the total variational distance
- (ii) For  $F_K = \{\chi_{(-\infty, t]} \mid t \in \mathbb{R}\}$  on  $\mathcal{X} = \mathbb{R}$ ,  $\text{IPM}[F, P, Q]$  is called the Kolmogorov /  $L^\infty$ -distance, the max-norm of their cumulative distributions.
- (iii) for metric space  $(\mathcal{X}, d)$  ( $\mathcal{A}_\mathcal{X} = \mathcal{B}(\mathcal{T}_d)$ ) and  $F_W = \{f \in L^0(\mathcal{X}, \mathbb{R}) \cap B(\mathcal{X}, \mathbb{R}) \mid \|f\|_L := \sup_{x \neq y} \frac{|f(x) - f(y)|}{d(x, y)} \leq 1\}$ ,  $\text{IPM}[F_W, P, Q]$  is called earth mover / Wasserstein /  $L^1$ -distance

**Definition D.4** (Maximum Mean Discrepancy). Let  $(\mathcal{X}, \mathcal{A}_\mathcal{X})$  be a measurable space,  $(H \subseteq \mathbb{C}^\mathcal{X}, \langle \cdot, \cdot \rangle_H, k : \mathcal{X} \times \mathcal{X} \rightarrow \mathbb{C})$  a RKHS,  $P, Q \in \mathcal{M}^1(\mathcal{X}, \mathcal{A}_\mathcal{X})$  and  $\mathcal{H} = \{f \in H \mid \|f\|_H \leq 1\}$ . The integral probability metric  $\text{IPM}[\mathcal{H}, P, Q]$  is called maximum mean discrepancy (MMD), written

$$\begin{aligned} \text{MMD}_k[P, Q] &:= \text{IPM}[\mathcal{H}, P, Q] = \sup_{f \in \mathcal{H}} \left| \int_{\mathcal{X}} f(x) dP(x) - \int_{\mathcal{X}} f(x) dQ(x) \right| \\ &= \sup_{f \in \mathcal{H}} |\langle f, \mu_P - \mu_Q \rangle_H| = \|\mu_P - \mu_Q\|_H \end{aligned}$$

where we used  $f(x) = \langle f, k(\cdot, x) \rangle_H$ .

*Remark D.5* (Expression of MMD, definiteness). Note:

(i) We can express the MMD in terms of kernel  $k$  as

$$\text{MMD}_k^2[P, Q] = \|\mu_P - \mu_Q\|_H^2 = \mathbb{E}_{X, X'}[k(X, X')] - 2\mathbb{E}_{X, Y}[k(X, Y)] + \mathbb{E}_{Y, Y'}[k(Y, Y')]$$

where  $X, X' \sim P, Y, Y' \sim Q$  independent, and we use

$$\begin{aligned} \|\mu_P\|_H^2 &= \left\langle \int k(\cdot, x') dP(x'), \int k(\cdot, x) dP(x) \right\rangle_H = \iint \langle k(\cdot, x'), k(\cdot, x) \rangle_H dP(x') dP(x) \\ &= \mathbb{E}_{X, X'}[k(X, X')] \end{aligned}$$

(ii) If  $H$  resp.  $k$  characteristic, the MMD is definite, meaning

$$\text{MMD}_k[P, Q] = 0 \Leftrightarrow P = Q$$

## E. Experimental Details

### E.1. Datasets

CANCER (GENG ET AL., 2017)

The cancer dataset is simulated using the lung cancer PK/PD model of Geng et al. (2017), which has been used extensively in longitudinal treatment-effect benchmarks.

**Dynamics.** The state is  $X_t = (V_t, C_t) \in \mathbb{R}_+^2$ , where  $V_t$  denotes tumor volume and  $C_t$  denotes the chemotherapy drug concentration. The control is  $U_t = (U_{c,t}, U_{r,t}) \in \mathbb{R}_+^2$ , where  $U_{c,t}$  is the administered chemotherapy dose and  $U_{r,t}$  is the radiotherapy dose.

Tumor volume evolves according to an ODE with multiplicative noise,

$$\frac{dV}{dt} = \left( \rho \log\left(\frac{K}{V(t)}\right) - \beta_c C(t) - (\alpha_r U_r(t) + \beta_r U_r(t)^2) + e_t \right) V(t), \quad (13)$$

where  $e_t \sim \mathcal{N}(0, \sigma^2)$ . Equivalently, this can be written as the SDE

$$dV_t = \left[ \rho \log\left(\frac{K}{V_t}\right) - \beta_c C_t - \alpha_r U_{r,t} - \beta_r U_{r,t}^2 \right] V_t dt + \sigma V_t dW_t, \quad (14)$$

with standard Brownian motion  $W_t$ . We set  $(\rho, K, \beta_c, \alpha_r, \beta_r)$  to the mean values of the prior distribution reported by [Geng et al. \(2017\)](#) and fix the noise scale to  $\sigma = 0.1$  in our simulations.

The chemotherapy concentration follows exponential decay with input from administered chemotherapy:

$$\frac{dC}{dt} = -k_C C(t) + U_c(t), \quad (15)$$

where  $k_C = 0.5$ .

**Treatment Process.** For each simulated patient trajectory, we sample one of two treatment protocols inspired by ([Curran Jr et al., 2011](#); [Hess et al., 2023](#); [Vanderschueren et al., 2023](#)): *sequential* therapy (three weeks of weekly chemotherapy followed by three weeks of radiotherapy) or *concurrent* therapy (biweekly chemo–radiotherapy administration over six weeks). Treatments are modeled as bang-bang controls: at each dosing time  $t$ , chemotherapy is either off or delivered at a fixed dose,  $U_{c,t} \in \{0, 5\}$  (mg), and radiotherapy is either off or delivered at a fixed fraction dose,  $U_{r,t} \in \{0, 2\}$  (Gy), where Gy denotes Gray (ionizing radiation dose).

**Initial State.** Following [Geng et al. \(2017\)](#), we first sample a cancer stage and then sample the initial tumor volume  $V_0$  from the corresponding stage-conditional prior defined in [Geng et al. \(2017\)](#). The initial chemo concentration  $C_0$  is set to zero.

**Simulation and Preprocessing.** We generate 800 patient trajectories over a 60-day time window ( $t \in [0, 60]$ ) for training and sample 128 for validation purposes. To induce irregular observation patterns, we randomly mask 30% of observations uniformly at random. We apply a log-transform to the state variables and then standardize (zero mean, unit variance) using statistics computed on the training set only. Controls are min–max normalized to  $[0, 1]$  using the known dose bounds.

COVID-19 ([DAI ET AL., 2021](#); [QIAN ET AL., 2021](#))

We use the COVID-19 disease progression simulator under dexamethasone treatment proposed by [Qian et al. \(2021\)](#) (adoption of [Dai et al. \(2021\)](#)). The simulator describes the interaction between disease progression and immune response, coupled with a treatment/exposure component.

**Dynamics.** The original simulator in [Qian et al. \(2021\)](#) is specified as a deterministic ODE system. To model stochasticity and unobserved heterogeneity, we augment the dynamics with additive diffusion terms, yielding the following SDE formulation with state  $X_t = (X_{1,t}, X_{2,t}, X_{3,t}, X_{4,t})$ . The state variables  $X_{1,t}, X_{2,t}, X_{3,t}, X_{4,t}$  represent viral load, innate immune response to viral infection, adaptive immunity, and (effective) dexamethasone concentration in lung tissue, respectively:

$$\begin{aligned} dX_{1,t} &= \left( k_{dp} X_{1,t} - k_{di} X_{1,t} X_{3,t}^{h_c} - k_{dr} X_{1,t} X_{2,t} \right) dt + \sigma_1 X_{1,t} dW_t^1, \\ dX_{2,t} &= \left( k_{id} X_{1,t} - k_{io} X_{2,t} + k_{if} X_{1,t} X_{2,t} + \frac{k_{ep} X_{2,t}^{h_p}}{k_{cp} + X_{2,t}^{h_p}} - k_d X_{4,t} X_{2,t} \right) dt + \sigma_2 X_{2,t} dW_t^2, \\ dX_{3,t} &= (k_{im} X_{2,t}) dt + \sigma_3 X_{3,t} dW_t^3, \\ dX_{4,t} &= (k_{kel} U_{c,t} - k_{kel} X_{4,t}) dt + \sigma_4 X_{4,t} dW_t^4. \end{aligned}$$

Here,  $W_t^i$  denote independent standard Wiener processes and we set  $\sigma = \sigma_i = 0.1$  for  $i \in \{1, 2, 3, 4\}$ . The dynamics parameters are positive real numbers and described in [Qian et al. \(2021\)](#); [Dai et al. \(2021\)](#). Following [Qian et al. \(2021\)](#) we set the coefficients  $h_p = h_c = 2$  and the rest to one.

The signal  $U_{c,t}$  denotes our control variable and represents the exogenous dexamethasone administration/exposure input.

**Treatment Process.** We consider a single-intervention setting over a 14-day horizon. Dexamethasone is administered at one of three predefined intervention times,  $t \in \{t_1, t_2, t_3\}$ . Concretely, for each simulated trajectory we sample an intervention time  $t^* \in \{t_1, t_2, t_3\}$  and a dosage  $d \sim \text{Unif}(0, 10)$  mg and define the control signal as an exponential decay

$$U_c(t) = d \cdot \mathbb{I}(t \geq t^*) \exp(-k_{kel}(t - t^*)).$$

**Initial State.** We sample initial conditions  $X_0$  from an exponential distribution with rate  $\lambda = 100$ , as described in Qian et al. (2021).

**Simulation and Preprocessing.** In total we sample 500 trajectories over a 14-day horizon. We sample 5 trajectories per initial condition and treatment. State trajectories are standardized using statistics computed on the training set (zero mean and unit variance per dimension). Treatment inputs are min–max normalized to  $[0, 1]$  using the known dose bounds  $d \in [0, 10]$ . Validation trajectories consist of 480 trajectories sampled in the same way.

## E.2. Treatment Optimization Objectives

We consider three treatment optimization objectives, two for the cancer simulator and one for the Covid-19 simulator. In all cases, we optimize over admissible treatment plans  $U \in \mathcal{U}$  and evaluate objectives under the (stochastic) simulator dynamics, hence the expectation with respect to the driving noise.

**Cancer – Explicit Target State.** Let  $X_t = (V_t, C_t)$  denote the cancer state, where  $V_t$  is tumor volume. Given an initial patient state  $V_{t_0} = v_0$  and initial concentration  $C_{t_0} = 0$ , we seek a treatment plan that minimizes terminal tumor volume while regularizing treatment intensity:

$$\min_{u \in \mathcal{U}} \mathbb{E} \left[ \int_{t_0}^{t_f} \lambda_c u_{c,t}^2 + \lambda_r u_{r,t}^2 dt + V_{t_f}^2 \mid X_{t_0} = (v_0, 0) \right], \quad t_f = 60, \quad (16)$$

where  $\lambda_c = \lambda_r = 10^{-3}$  in our experiments.

**Cancer – Relative Target State.** In the second cancer objective, given an initial patient state  $V_{t_0} = v_0$  and  $C_{t_0} = 0$ , the goal is to achieve a prescribed *relative* reduction in tumor volume at the terminal time. We define the relative target  $v^* := 0.3 v_0$ , corresponding to a 70% reduction from the initial state. We minimize the deviation from this target while regularizing treatment intensity:

$$\min_{u \in \mathcal{U}} \mathbb{E} \left[ \int_{t_0}^{t_f} \lambda_c u_{c,t}^2 + \lambda_r u_{r,t}^2 dt + (V_{t_f} - v^*)^2 \mid X_{t_0} = (v_0, 0) \right], \quad t_f = 60, \quad (17)$$

with  $\lambda_c = \lambda_r = 10^{-3}$ .

**COVID-19 – Target Trajectory.** Let  $X_t \in \mathbb{R}^{d_x}$  denote the COVID-19 simulator state and let  $u_t \in \mathbb{R}^{d_u}$  denote the (one-dimensional) dexamethasone exposure control. Given an initial condition  $X_{t_0} = x_0$ , we define a target trajectory  $X_t^*$  over  $[t_0, t_f]$  by sampling  $M$  trajectories  $\{X^{(m)}\}_{m=1}^M$  from the data-generating process (including initial conditions) and averaging pointwise in time  $X_t^* := \frac{1}{M} \sum_{m=1}^M X_t^{(m)}$ ,  $t \in [t_0, t_f]$ . We then optimize treatment to track  $X^*$ :

$$\min_{u \in \mathcal{U}} \mathbb{E} \left[ \int_{t_0}^{t_f} \lambda_x \|X_t - X_t^*\|_2^2 dt \mid X_{t_0} = x_0 \right]. \quad (18)$$

We choose a factor of  $\lambda_x = \frac{1}{1000}$  so that the regularization strength of our regularizer can live on the same scale as for the Cancer task. When reporting the costs, we choose  $\lambda_x = 1$

For all tasks, we solve the problem 15 times corresponding to 15 different initial conditions. For the Cancer tasks, we sample from the same initial state prior distribution as the training dataset and restrict ourselves to initial tumors with a diameter between 2 and 5cm. For the Covid task, we sample 15 initial conditions from the same prior distribution as the training dataset and then 15 treatment trajectories from the same prior used for the training dataset. Then, the target trajectory is obtained by sampling and then averaging 20 trajectories for each (treatment, initial condition) pair.

### E.3. Treatment Function Parameterization

We solve the treatment optimization problem using a direct single-shooting approach. For details on numeric approaches to solving continuous-time optimal control problems, we refer to (Gros & Diehl, 2020). We parameterize the control function  $u(t)$  (denoted by  $u(t, q)$ ) with the parameter  $\phi$ .

Specifically, for the Cancer tasks where we have a two-dimensional control consisting of the chemo- and radiotherapy treatment, we parameterize the chemo parameters  $\phi_c = [\phi_{c,timepoints}, \phi_{c,dosage}]$ , with  $\phi_{c,timepoints}$  denoting the timepoints of treatment administration, and  $\phi_{c,timepoints}$  the respective dosages. Similarly we parameterize the radiotherapy parameters  $\phi_r$ . We restrict the controls to a maximum of  $K$  treatment administrations for chemo- and radiotherapy, respectively. Now, to obtain a control function from our parameters, we model the control similarly to the data generating process and model the control function  $u_{chemo}(t)$  by modeling a bang-bang control and setting  $u_{chemo}(t) = \sum_{i=1}^K \mathbb{I}_{(t \in [\phi_{c,timepoints,i}, \phi_{c,timepoints,i+1})} \cdot \phi_{c,dosage,i}$ , where  $\mathbb{I}$  is the indicator function. The function  $u_{radio}(t)$  is constructed similarly.

Second, for the Covid task, we have a one-dimensional control corresponding to the Dexamethasone administration. Again, we use a similar parameterization corresponding to the timepoints and the corresponding dosage  $\phi = [\phi_{timepoints}, \phi_{dosage}]$ . Again, we restrict the treatment trajectory to a maximum of  $K$  treatments administrations. In the Covid simulator, the control variable is defined with an exponential decay. Thus, we obtain the control function from our parameters by modeling  $u(t) = \sum_{i=1}^K \phi_{dosage,i} \cdot \mathbb{I}_{t > \phi_{dosage,i}} \cdot \exp(t_i - t)$ .

### E.4. Practical Implementation Details of Our Approach

#### NEURAL SDE

We model the drift and diffusion of the SDE with neural networks  $\mu_\theta : \mathbb{R}^{d_y} \times A \rightarrow \mathbb{R}^{d_y}$ ,  $\sigma_\theta : \mathbb{R}^{d_x} \times A \rightarrow \mathbb{R}^{d_x \times d_w}$  and  $\zeta_\theta : \mathbb{R}^{d_\nu} \rightarrow \mathbb{R}^{d_x}$  to model the strong solution  $\hat{X} : I \rightarrow \mathbb{R}^{d_x}$  of

$$d\hat{X}_t = \mu_\theta(\hat{X}_t, U_t)dt + \sigma_\theta(\hat{X}_t, U_t)dW_t, \quad \hat{X}_0 = \zeta_\theta(V), \quad V \sim \mathcal{N}(0, I_{d_\nu}) \quad (19)$$

$W : I \rightarrow \mathbb{R}^{d_w}$  is a  $d_w$ -dimensional Brownian motion and  $U = (U_t)_{t \in I}$  our control.

In all experiments, we parameterized the drift and diffusion so that each state has its own independent neural networks. Each drift neural network consists of a three-layer fully-connected neural network with 64 hidden units, while the diffusion networks consist of a one-layer fully-connected neural network with 8 hidden units. We use LipSwish-activation function for intermediate layers and tanh-activation for the final layers. We optimize the neural SDE using a signature-kernel score objective (see below, based on Issa et al. (2023)). For training we use the RMSProp optimizer with a learning rate of 0.0001 and 0.001 for the Cancer and Covid dataset respectively. We optimize over 15000 and 30000 gradient steps, where each gradient step has a batch size of 16 trajectories.

**Signature score for training neural SDEs** Here, we detail how we adapt the signature score training method by Issa et al. (2023) to our conditional training as we have samples from the treatment process and the state process. Issa et al. (2023) propose a non-adversarial training objective for neural SDEs based on the signature kernel: The signature kernel score of  $P \in \mathcal{M}^1(\mathcal{X}, \mathcal{B}(\mathcal{T}_\mathcal{X}))$  and  $y \in \mathcal{X}$  is the map  $\Phi_{\text{sig}} : \mathcal{M}^1(\mathcal{X}, \mathcal{B}(\mathcal{T}_\mathcal{X})) \times \mathcal{X} \rightarrow \mathbb{R}$  defined by

$$\Phi_{\text{sig}}(P, y) := \mathbb{E}_{x, x' \sim P} [k_{\text{sig}}(x, x')] - 2 \mathbb{E}_{x \sim P} [k_{\text{sig}}(x, y)].$$

$\Phi_{\text{sig}}$  is a strictly proper score, meaning it assigns the lowest expected score when the proposed prediction is realized by the true probability distribution. Let  $(\Omega, \mathcal{F}, P)$  be a probability space,  $T > 0$ ,  $d_x \in \mathbb{N}$ . For path-space

$$\mathcal{X} := \{ \gamma \in C_{\text{BV}}([0, T], \mathbb{R}^{d_x}) \mid \exists i \in [d] : \gamma^i \text{ monotone} \},$$

Let  $\mathcal{T}$  be a topology such that the signature kernel  $k_{\text{sig}} : \mathcal{X} \times \mathcal{X} \rightarrow \mathbb{R}$  is continuous. Let  $X^{\text{true}} : \Omega \rightarrow \mathcal{X}$  be a random variable with sample  $\{x^{(i)}\}_{i=1}^N \stackrel{iid}{\sim} P_{X^{\text{true}}} \in \mathcal{M}^1(\mathcal{X}, \mathcal{B}(\mathcal{T}_\mathcal{X}))$ .

In the unconditional setting (as described in Issa et al. (2023)), one can learn a neural SDE  $X^\theta$  into  $\mathcal{X}$  such that its law  $P_{X^\theta} \approx P_{X^{\text{true}}}$ , use the training objective

$$\min_{\theta} \mathcal{L}(\theta), \quad \mathcal{L}(\theta) := \mathbb{E}_{y \sim P_{X^{\text{true}}}} [\Phi_{\text{sig}}(P_{X^\theta}, y)],$$

which is equivalent to optimization using  $\text{MMD}_{k_{\text{sig}}}^2 [P_{X^\theta}, P_{X^{\text{true}}}]$  as the last term  $\mathbb{E}_{y, y' \sim P_{X^{\text{true}}}} [k_{\text{sig}}(y, y')]$  is constant w.r.t.  $\theta$ .

However, our neural SDE is a conditional setting, since we observe both a treatment process and a state process. Given a distribution  $P_Z$  to condition on,  $P_{X^{\text{true}}|Z}(\cdot | z)$ ,  $z \sim P_Z$  the target conditional distribution with sample  $\{(z^{(i)}, x^{(i)})\}_{i \in [N]}$ ,  $z^{(i)} \sim P_Z$ ,  $x^{(i)} \sim P_{X^{\text{true}}|Z}(\cdot | z^{(i)})$ . To learn a neural SDE  $X^\theta$  into  $\mathcal{X}$  such that  $P_{X^\theta}(\cdot | z) \approx P_{X^{\text{true}}}(\cdot | z)$ , train with the modified objective:

$$\min_{\theta} \mathcal{L}'(\theta), \quad \text{where} \quad \mathcal{L}'(\theta) := \mathbb{E}_{z \sim P_Z} [\mathbb{E}_{x \sim P_{X^{\text{true}}|Z}(\cdot | z)} [\Phi_{\text{sig}}(P_{X^\theta}(\cdot | z), x)]] .$$

Thus, in our controlled SDE setting, we have to adapt the above conditional objective in the following way. Given a control signal  $u$  to condition on, the target conditional distribution  $P_{X^{\text{true}}|U}(\cdot | u)$  with sample  $\{(u^{(i)}, x^{(i)})\}_{i \in [N]}$ ,  $u^{(i)} \sim P_U$ ,  $x^{(i)} \sim P_{X^{\text{true}}|U}(\cdot | u^{(i)})$ . To learn a neural SDE  $X^\theta$  into  $\mathcal{X}$  such that  $P_{X^\theta}(\cdot | u, x_0) \approx P_{X^{\text{true}}}(\cdot | u, x_0)$ , train with the modified objective:

$$\min_{\theta} \mathcal{L}'(\theta), \quad \text{where} \quad \mathcal{L}'(\theta) := \mathbb{E}_{u \sim P_U, x_0 \sim P_{X_0}} [\mathbb{E}_{x \sim P_{X^{\text{true}}}(\cdot | u, x_0)} [\Phi_{\text{sig}}(P_{X^\theta}(\cdot | u, x_0), x)]] .$$

In all of our experiments, we use an RBF-lifting kernel with a smoothing parameter  $\sigma = 1$  to compute the above loss. We set the order of dyadic refinement associated to the PDE solver for computing the signature kernel to 1. Following Issa et al. (2023), we apply a time-normalization transform and augment true and predicted paths with the normalized-time component before passing them through the loss function.

#### TREATMENT PLAN OPTIMIZATION

**Signature-Kernel Based Regularizer.** We compute the MCMD regularizer using the respective validation dataset together with an RBF-lifting kernel with smoothing parameter  $\sigma = 1$ . Again, we use a dyadic refinement factor 1 for the PDE solver and apply a time-normalization transform and augment true and predicted paths with the normalized-time component before evaluating the path. For the initial condition, we also use an RBF-kernel with smoothing parameter  $\sigma = 1$ .

**Optimization Procedure** We use the parameterized representation of the control functions described in Appendix E.3. This allows for direct single-shooting control optimization. We initialize the timepoint parameters  $\phi_{\text{timepoints}}$  by uniformly sampling over the time interval  $I$ . The dosage parameters  $\phi_{\text{dosage}}$  are initialized by uniformly sampling between  $[0.1, 0.3]$ . We use gradient-descent based methods (RMSProp optimizer) with a learning rate of 0.001 for both Cancer tasks and a learning rate of 0.01 for the Covid task. All tasks are optimized with 5000 gradient-update steps. Moreover, we use Monte Carlo sampling with a sample size = 10 to approximate the expectation in our objective function  $\mathcal{J}$ .

**Ours (rank)** When we report the Spearman correlation (to compare with the benchmark methods), we rely on the same control library. There, we simply use our trained neural SDE to predict the costs for the respective candidate controls. We do not use a regularization for these settings.

#### E.5. Baseline Methods

**TE-CDE (Seedat et al., 2022).** In our experiments, we use the same model architecture as proposed in the original paper, meaning a 2-layer neural network with hidden state dimension 128 for both the neural CDE encoder and decoder. We train the decoder already to predict the same time horizon as needed in our control tasks. We also adjust the balancing-representation loss objective from a cross-entropy loss to a mean-squared-error loss as it naturally extends to our general formulation of continuous-valued treatments. We perform a grid-search for selecting the learning rate  $\in \{0.0001, 0.001, 0.01\}$ , number of epochs  $\in \{50, 100\}$  and dimensions of the latent state  $\in \{8, 16\}$ . The optimal hyperparameters are determined by choosing the set that results in the lowest mean squared error on the validation dataset, for the Cancer and Covid datasets, respectively.

**INSITE/SINDy. (Kacprzyk et al., 2024; Brunton et al., 2016a)** INSITE is a framework for bridging treatment effect estimation and dynamical system discovery. Following Kacprzyk et al. (2024), we also instantiate the INSITE framework using SINDy (Brunton et al., 2016a). Importantly, since we do not have patient heterogeneity in our experiments (so where each patient has their ‘‘own’’ dynamics parameters) and instead model patient-conditioned effects by conditioning on the observed history, we only obtain the population-level dynamics equation and not further fine-tune it on a specific trajectory.

Moreover following (Kacprzyk et al., 2024), we incorporate the continuous-valued treatment directly as a control input and use SINDy with control. SINDy works as follows: Assuming that the target symbolic expression  $f$  is a linear combination of library functions from  $L \subset \text{Funct}(\mathbb{R}^{d_x}, \mathbb{R}^{d_y})$  ( $f = \sum \theta_i h_i$  or  $\text{span}(L) = \mathcal{F}$ ), linear symbolic regression solves the multivariate, multidimensional SR - problem ( $\mathcal{F} \subseteq \text{Funct}(\mathbb{R}^{d_x}, \mathbb{R}^{d_y})$ ,  $\mathcal{D} = \{(x_i, y_i)\}_{i \in [n]}$ ,  $x_i \in \mathbb{R}^{d_x}$ ,  $y_i \in \mathbb{R}^{d_y}$ ) by:

1. Assign each  $f_j \in L$  a coefficient vector  $\theta_j \in \mathbb{R}^{d_y}$  with  $\theta_0 \in \mathbb{R}^{d_y}$  s.t.

$$y = \sum_{j=1}^k f_j(x) \theta_j + \theta_0 \quad (\text{A})$$

- (ii) Apply (A) to all input - output pair to obtain a system of linear equations, that can be written in matrix-form as

$$\underbrace{\begin{pmatrix} y_1^\top \\ y_2^\top \\ \vdots \\ y_n^\top \end{pmatrix}}_Y = \underbrace{\begin{pmatrix} 1 & f_1(x_1) & f_2(x_1) & \cdots & f_k(x_1) \\ 1 & f_1(x_2) & f_2(x_2) & \cdots & f_k(x_2) \\ \vdots & \vdots & \vdots & \cdots & \vdots \\ 1 & f_1(x_n) & f_2(x_n) & \cdots & f_k(x_n) \end{pmatrix}}_{U(X)} \underbrace{\begin{pmatrix} \theta_0^\top \\ \theta_1^\top \\ \vdots \\ \theta_k^\top \end{pmatrix}}_\Theta \quad (\text{B})$$

or more compact as  $Y = U(X) \cdot \Theta$  where  $U := U(X) \in \mathbb{R}^{n \times (k+1)}$  the library functions evaluated on input data and  $\Theta \in \mathbb{R}^{(k+1) \times d_y}$  the (sparse) matrix of coefficients.

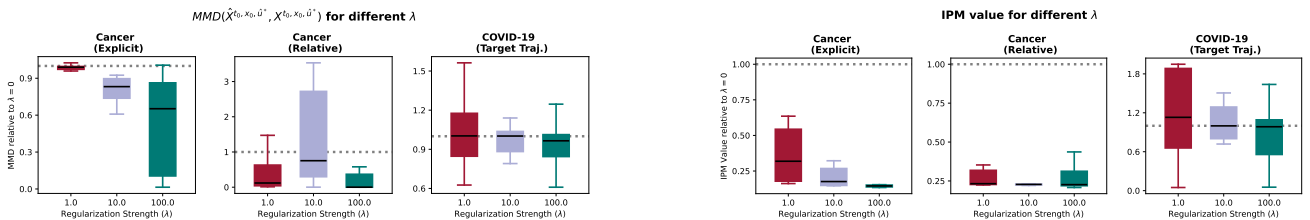
- (iii) Solve (B) with  $\Theta = (U^\top U)^\dagger U^\top Y$

*Remark E.1.* The above describe SINDy-framework is extend to control inputs (SINDy with control; see Brunton et al. (2016b)) by augmenting the library of functions in  $(x, u)$  and fitting the dynamics  $\dot{x} = f(x, u)$ ,

In order to establish a fair comparison with the SINDy baseline, similar to Kacprzyk et al. (2024), we used the STLSQ optimizer together with the polynomial library (instead of the wSINDy weak-form library) and performed hyperparameter-tuning over the polynomial degree  $\text{deg} \in \{1, 2\}$ , threshold  $\{0.1, 0.2, 0.5\}$  and the ridge regularization parameter  $\lambda \in \{0.1, 0.2, 0.5\}$ .

**Library of Candidate Controls.** The library of candidate controls consists of 100 control candidates. We randomly sample the parameters  $\phi$  which parameterize the continuous-time control function. For the respective problems, we use the parameterization described in Appendix E.3. We initialize the treatment timepoints  $\phi_{\text{timepoints}}$  by uniformly sampling over the time interval of interest  $[t_0, t_f]$ . The dosages are obtained by randomly sampling over the interval  $[0, 1]$  (in the min-max-normalized control space). For the Cancer tasks, we choose a maximum of  $K = 5$  treatment administrations. For the Covid task, we chose  $K = 1$  treatment mirroring the fact that the target trajectory was also generated with a single treatment administration.

## F. Additional Results



(a)  $\text{MMD}_{k_{\text{sig}}}$  between the true and predicted patient trajectory distribution for the optimal control obtained with different levels of regularization strength  $\lambda$ . This figure shows the Signature-Kernel-Score.

(b)  $\text{MCMD}_{k_{\text{sig}}}$  estimator for the optimal control obtained with different levels of regularization strength  $\lambda$ .

Figure 3. Effects of regularization strength parameter  $\lambda$ .